© 2020. Published by The Company of Biologists Ltd | Journal of Cell Science (2020) 133, jcs240085. doi:10.1242/jcs.240085

RESEARCH ARTICLE

FAT10 localises in dendritic cell aggresome-like induced structures and contributes to their disassembly

Richard Schregle[1,*], Stefanie Mueller[1,*], Daniel F. Legler[2], Jérémie Rossy[2], Wolfgang A. Krueger[3] and Marcus Groettrup[1,2,‡]

ABSTRACT

Dendritic cell (DC) aggresome-like induced structures (DALIS) are protein aggregates of polyubiquitylated proteins that form transiently during DC maturation. DALIS scatter randomly throughout the cytosol and serve as antigen storage sites synchronising DC maturation and antigen presentation. Maturation of DCs is accompanied by the induction of the ubiquitin-like modifier FAT10 (also known as UBD), which localises to aggresomes, structures that are similar to DALIS. FAT10 is conjugated to substrate proteins and serves as a signal for their rapid and irreversible degradation by the 26S proteasome similar to, yet independently of ubiquitin, thereby contributing to antigen presentation. Here, we have investigated whether FAT10 is involved in the formation and turnover of DALIS, and whether proteins accumulating in DALIS can be modified through conjunction to FAT10 (FAT10ylated). We found that FAT10 localises to DALIS in maturing DCs and that this localisation occurs independently of its conjugation to substrates. Additionally, we investigated the DALIS turnover in FAT10-deficient and -proficient DCs, and observed FAT10-mediated disassembly of DALIS. Thus, we report further evidence that FAT10 is involved in antigen processing, which may provide a functional rationale as to why FAT10 is selectively induced upon DC maturation.

KEY WORDS: DALIS, FAT10, Ubiquitin, Dendritic cells, Proteasome

INTRODUCTION

Ubiquitylation sustains a plethora of different functions within the innate and adaptive immune system. It has regulatory functions in T cell selection and differentiation, in T and B cell activation, and in the maturation of dendritic cells (DCs). Additionally, it is involved in pathogen clearance, immune evasion by pathogens, and autoimmunity (Hu and Sun, 2016; Li et al., 2016). Besides the conjugation of ubiquitin, attachment of other ubiquitin-like modifiers (UBLs), such as ISG15 or SUMO proteins, is involved in the regulation of the immune system (Liu et al., 2013; Oudshoorn et al., 2012). The ubiquitin-like modifier 'HLA-F adjacent transcript 10' [FAT10; also known as ubiquitin D (UBD)] is strongly associated with the immune system. FAT10 was identified 24 years ago, and its expression was initially found to be confined to mature DCs and B cells (Fan et al., 1996; Bates et al., 1997). Since then FAT10 has emerged as the only UBL, aside from ubiquitin, which targets its covalently bound substrates for degradation by the 26S proteasome in a ubiquitin-independent manner (Hipp et al., 2005; Raasi et al., 2001; Schmidtke et al., 2009). Similar to ubiquitin and other UBLs, substrate proteins are modified covalently by FAT10 (FAT10ylation) in a process mediated by an E1-activating enzyme, UBA6 (Jin et al., 2007; Pelzer et al., 2007), an E2-conjugating enzyme, USE1 (Gu et al., 2007), and most likely by E3-ligating enzymes, which remain to be discovered. Interestingly, this conjugation machinery is bispecific for FAT10 and ubiquitin (Aichem et al., 2010; Chiu et al., 2007). Moreover, FAT10 is expressed with a free diglycine motif at its C-terminus unlike other UBLs, which require post-translational processing to expose their C-terminal diglycine motif (Kerscher et al., 2006; Raasi et al., 2001). Apart from being covalently conjugated to substrate proteins, FAT10 can interact non-covalently with proteins, as has been shown for histone deacetylase 6 (HDAC6), through which FAT10 gets targeted to aggresomes (Kalveram et al., 2008), or the autophagy adaptor p62 (also known as SQSTM1), which colocalises with FAT10 in p62 bodies (Aichem et al., 2012). FAT10 is synergistically inducible by the pro-inflammatory cytokines TNF and IFN-γ in virtually all cells (Liu et al., 1999; Lukasiak et al., 2008; Raasi et al., 1999), but is also upregulated during DC maturation triggered by different TLR ligands (Bates et al., 1997; Ebstein et al., 2009; Lukasiak et al., 2008). Interestingly, FAT10 expression under non-inflammatory conditions is confined to tissues or specific cells of the immune system (Bates et al., 1997; Buerger et al., 2015; Canaan et al., 2006; Ebstein et al., 2009; Lee et al., 2003; Ocklenburg et al., 2006; Schregle et al., 2018). FAT10 is involved in antigen processing and presentation since it labels protein antigens for their proteasomal degradation and consequently for antigen presentation (Ebstein et al., 2012; Schliehe et al., 2012). Aside from this, FAT10 might play a role in the defence against intracellular bacteria, as FAT10 has been shown to coat cytosolic *Salmonella typhimurium* and to promote resistance against these bacteria in mice (Spinnenhirn et al., 2014). Additionally, FAT10 plays a role in the antiviral immune response by regulating the secretion of type I and type II interferons by activated $CD8^+$ T cells (Mah et al., 2019).

DCs are the most potent antigen-presenting cells and link the innate and adaptive immune system (Mellman, 2013). For efficient presentation of peripheral antigens, DCs transiently accumulate ubiquitylated proteins in cytosolic aggregates during their maturation (Lelouard et al., 2002). Analysis of these aggregates shows that they are similar to, yet distinct from aggresomes; hence, they are termed dendritic cell aggresome-like induced structures (DALIS) (Pierre, 2005). Contrary to the large aggresome, that forms

[1]Division of Immunology, Department of Biology, University of Konstanz, D-78457 Konstanz, Germany. [2]Biotechnology Institute Thurgau at the University of Konstanz, CH-8280 Kreuzlingen, Switzerland. [3]Klinikum Konstanz, D-78464 Konstanz, Germany.
*Present address: Biotechnology Institute Thurgau at the University of Konstanz, CH-8280, Kreuzlingen, Switzerland

‡Author for correspondence (Marcus.Groettrup@uni-konstanz.de)

D.F.L., 0000-0001-8610-4764; J.R., 0000-0002-5128-5283; M.G., 0000-0002-5423-6399

Handling Editor: John Heath
Received 2 October 2019; Accepted 4 June 2020

Journal of Cell Science (2020) 133, jcs240085. doi:10.1242/jcs.240085

at the microtubule-organising centre (MTOC) after several hours of proteasome inhibition and contains aggregated ubiquitylated or FAT10ylated proteins (Johnston et al., 1998; Kalveram et al., 2008), the smaller DALIS neither localise to the MTOC nor are they surrounded by the intermediate filament protein vimentin. DALIS are transient aggregates of ubiquitylated proteins that form independently of the microtubule network and do not affect proteasome activity (Lamark and Johansen, 2012; Lelouard et al., 2002). Aside from DCs, structures similar to DALIS termed 'ALIS' (Szeto et al., 2006; Wenger et al., 2012) or 'p62 bodies' (Bjørkøy et al., 2005) have been identified in macrophages (Canadien et al., 2005; Kettern et al., 2011) and non-professional antigen-presenting cells, but do not appear in activated B cells (Cenci et al., 2006). DALIS emerge and disappear in a biphasic process with an accumulation or aggregation phase during early stages of DC maturation and a presentation or degradation phase during late stages of maturation. This process is regulated by the Hsc/Hsp70 chaperone/co-chaperone machinery feeding the accumulated proteins into both the proteasomal and autophagic degradation pathway (Kettern et al., 2011). Interestingly, this regulatory machinery and proteasomes do not localise to DALIS under normal conditions (Herter et al., 2005; Lelouard et al., 2002). By contrast, enzymes of the ubiquitin-conjugating machinery, such as UBE1 (E1 enzyme), UBC4 and UBC5 (E2 enzymes), and CHIP (E3 ligase) (Lelouard et al., 2004) are present in DALIS further distinguishing them from aggresomes (Kopito, 2000). In order to form and to maintain DALIS, constant protein biosynthesis is required (Lelouard et al., 2002), which is regulated during DC maturation and facilitates proper DC function and survival (Lelouard et al., 2007). DALIS function as storage compartments for potential antigenic polypeptides which mainly derive from newly synthesised proteins or defective ribosomal products (DRiPs) (Khan et al., 2001; Lelouard et al., 2002; Lelouard et al., 2004; Yewdell et al., 1996). Upon viral infection, maturing DCs also target long-lived viral proteins, such as influenza nucleoprotein or Coxsackievirus B3 VP1 protein, to DALIS thereby delaying their presentation on MHC class I (Herter et al., 2005; Rahnefeld et al., 2011). However, exogenously acquired proteins, which can feed into the cross-presentation pathway (Alloatti et al., 2016) do not accumulate in DALIS (Lelouard et al., 2002). Therefore, DCs accumulate endogenously expressed antigenic proteins in DALIS during maturation. This delays antigen processing and presentation of self-peptides or pathogen-derived peptides to allow DCs to acquire a fully mature phenotype, which in turn enables DCs to migrate into the T cell zone of secondary lymphoid organs where they induce a cellular immune response (Steinman and Nussenzweig, 2002).

Previously, it has been shown that FAT10 localises to aggresomes under proteasomal inhibition in an HDAC6-dependent manner (Kalveram et al., 2008) and that FAT10 is able to target viral antigens for degradation thereby promoting their presentation on MHC class I molecules (Ebstein et al., 2012; Schliehe et al., 2012). Additionally, FAT10 interacts with p62 (Aichem et al., 2012), which also accumulates in DALIS in DCs (Kondylis et al., 2013) and in ALIS in macrophages (Fujita et al., 2011). Furthermore, our group has recently shown that FAT10 can modify newly translated proteins (Spinnenhirn et al., 2017) that constitute the majority of polypeptides targeted to DALIS (Lelouard et al., 2002; Lelouard et al., 2004). Inspired by these findings, we investigated whether FAT10 localises to DALIS in DCs, and the functional consequences of FAT10 deficiency on formation, maintenance and clearance of DALIS. We found that FAT10 localises to DALIS in human and murine DCs and that this occurs independently of FAT10 conjugation to target proteins. Moreover, we showed that HDAC6 is dispensable for DALIS formation, which further distinguishes them from aggresomes. Finally, we provide evidence that FAT10 does not contribute to DALIS accumulation but instead promotes their resolution.

RESULTS

FAT10 localises to DALIS in human mature dendritic cells

FAT10 localises to cytosolic protein aggregates together with its interaction partners HDAC6 and p62 (Aichem et al., 2012; Kalveram et al., 2008). In addition, FAT10 can destabilise viral antigens and directly target them for proteasomal degradation (Ebstein et al., 2012; Schliehe et al., 2012), is encoded in the MHC class I locus (Fan et al., 1995; Fan et al., 1996) and is cytokine-inducible (Liu et al., 1999; Raasi et al., 1999). These properties suggest that FAT10 might be involved in antigen presentation (Basler et al., 2015). Furthermore, FAT10 expression is upregulated upon DC maturation (Ebstein et al., 2009; Lukasiak et al., 2008), during which ubiquitylated proteins transiently accumulate in DALIS (Argüello et al., 2016; Lelouard et al., 2002). These findings prompted the question whether FAT10 also localises to DALIS in maturing DCs and whether it is involved in the accumulation and turnover of DALIS.

To test whether human FAT10 localises to DALIS, DCs were generated from $CD14^+$ monocytes isolated from peripheral blood. Maturation of the immature monocyte-derived DCs (MoDCs) was induced on day six of *in vitro* differentiation with either a cytokine cocktail consisting of IL-1β, IL-6, TNF, and IFN-γ (referred to as TNF/IFN-γ or T/I) or with lipopolysaccharide (LPS), both in GM-CSF- and IL-4-containing medium. Immature and matured MoDCs were stained for ubiquitin or p62 to visualise DALIS, and additionally for FAT10 (Fig. 1A–C). The phenotype, proper maturation and viability of the MoDCs were assessed by surface staining using the pan-DC marker CD11c as well as the maturation markers CD83 and CD86, and by live/dead staining (Fig. 1D,E). CD11c was expressed on ∼90% of the cells and did not change during maturation. Surface expression of CD83 and CD86 was upregulated during maturation, most prominently at 24 h of maturation, and did not differ between MoDCs matured by treatment with cytokines or LPS stimulation. The viability was slightly reduced upon maturation (Fig. 1E). Furthermore, upregulation of *FAT10* expression during DC maturation, as reported by others (Ebstein et al., 2009; Lukasiak et al., 2008), was confirmed by quantitative (q)PCR (Fig. 1F). Thus, the MoDC preparations showed the proper DC phenotype upon maturation without extensive cell death and upregulation of *FAT10* expression. Ubiquitin – as well as p62-positive DALIS that colocalised with endogenous FAT10 – was detected at later stages of maturation (16 h and 24 h) in mature MoDCs. The detection of endogenous FAT10 protein upon maturation was reflected by the expression levels determined by qPCR (Fig. 1F). Moreover, FAT10 accumulated in DALIS in cytokine- as well as LPS-matured MoDCs (Fig. 1A–C, highlighted by insets). Interestingly, almost all DALIS identified by ubiquitin and p62 also contained FAT10, consistent with the hypothesis that FAT10 plays a general role in DALIS clearance during late stages of DC maturation. Unfortunately, the low number of MoDCs that efficiently formed DALIS, did not allow for a proper quantification of the numbers of FAT10- and ubiquitin- or p62-positive DALIS. The inefficiency of DALIS formation in human MoDCs has been reported before by Terawaki and colleagues, who observed almost no DALIS upon maturation at 8 h post-induction with LPS (Terawaki et al., 2015).

Journal of Cell Science (2020) 133, jcs240085. doi:10.1242/jcs.240085

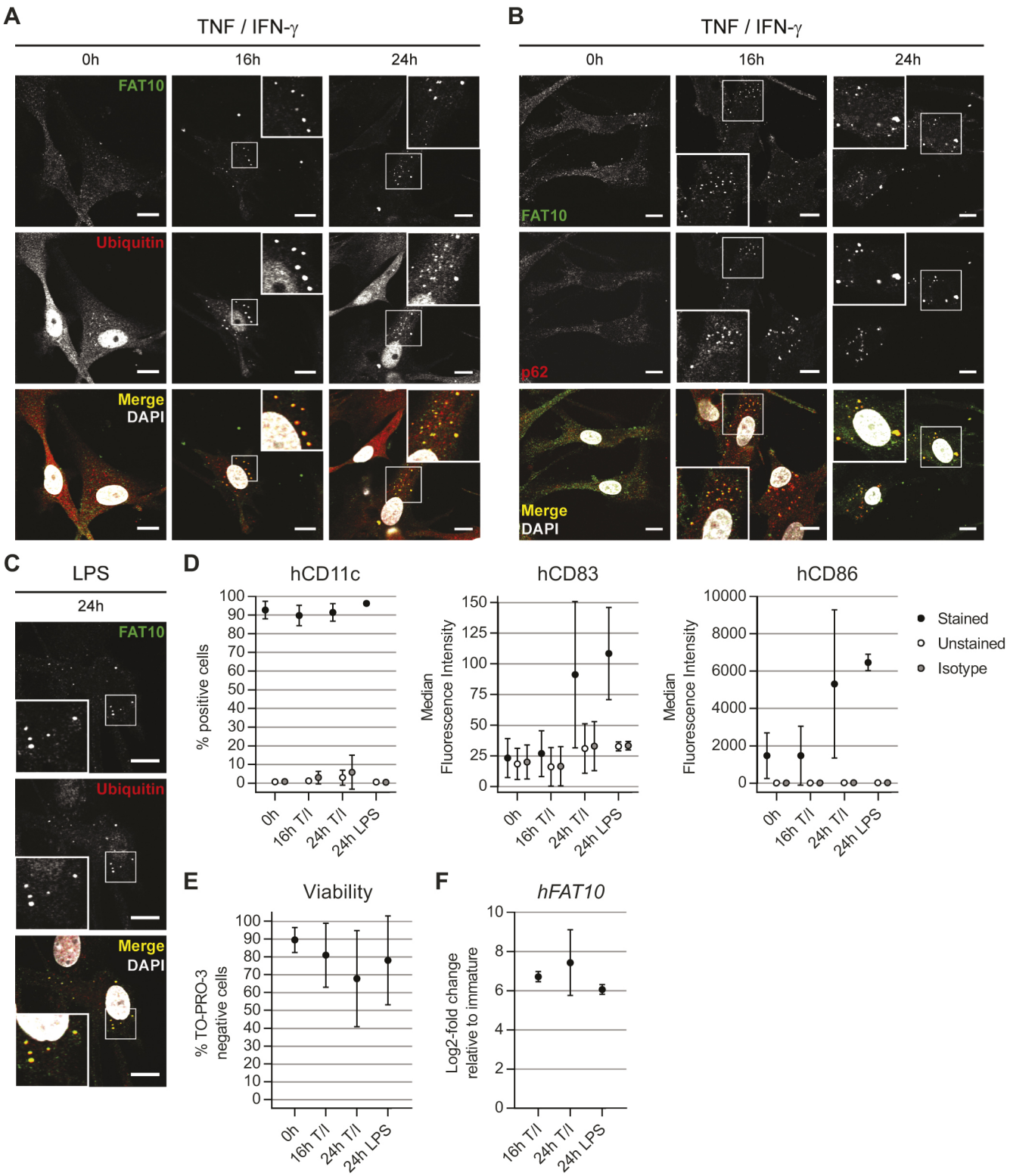

Fig. 1. Human FAT10 localises to DALIS in mature monocyte-derived DCs. MoDCs were differentiated from CD14$^+$ peripheral blood monocytes using GM-CSF and IL-4. (A–C) Maturation of MoDCs was induced using IL-1β, IL-6, TNF, and IFN-γ (referred to as TNF/IFN-γ in A,B, and T/I in D–F) and with LPS (C) in GM-CSF- and IL-4-containing medium for the indicated time points. After fixation, the cells were stained for FAT10 and ubiquitin (A,C) or p62 (B) prior to microscopy analysis. Insets highlight regions of interest where FAT10 and ubiquitin or p62 colocalise in DALIS. DAPI was used to stain nuclei. Representative images from two to five different MoDC preparations are shown. Scale bars: 10 µm. (D,E) MoDC preparations were analysed by flow cytometry. (D) Immature (0 h) and mature (16 h, 24 h T/I, and 24 h LPS) MoDCs were stained with antibodies against human (h)CD11c, hCD83 and hCD86 including isotype controls. (E) The viability of MoDCs was analysed using TO-PRO-3. (F) *hFAT10* mRNA expression levels determined by qPCR were normalised to *hGAPDH* and depicted as log2-fold change relative to immature MoDCs. Summarised data is shown in D–F obtained from two to five different MoDC preparations and is depicted as mean±s.d.

Journal of Cell Science (2020) 133, jcs240085. doi:10.1242/jcs.240085

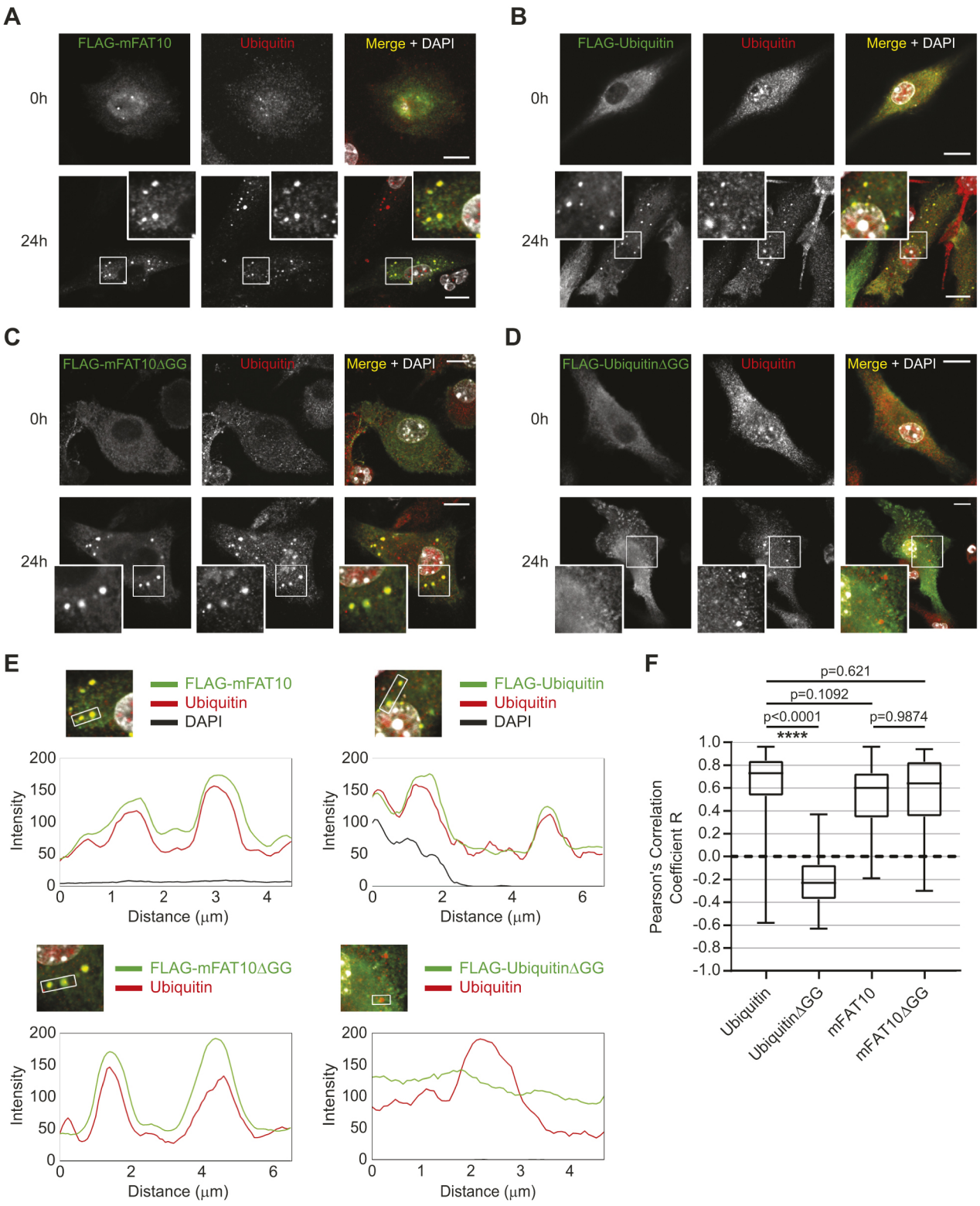

Fig. 2. See next page for legend.

FAT10 localises to DALIS in murine mature dendritic cells independently of conjugation

Next, localisation of murine FAT10 (mFAT10) to DALIS in bone marrow-derived dendritic cells (BMDCs) was analysed. Since, according to our experience, there is no mFAT10-reactive antibody available to date that is sensitive enough to visualise endogenous mFAT10, we established a lentiviral vector system to introduce FLAG-tagged mFAT10 into BMDCs. We observed no difference in DALIS formation between mock- and vehicle-transduced mature BMDCs as judged from confocal images of immature and mature *FAT10*-deficient (KO BMDC) and -proficient (wild-type; WT BMDC) BMDCs (Fig. S1A,B). Expression of *FLAG-mFAT10* and

Journal of Cell Science (2020) 133, jcs240085. doi:10.1242/jcs.240085

Fig. 2. Murine FAT10 accumulates in DALIS formed in murine mature DCs. (A–D) BMDCs were generated, and progenitor cells were transduced on day 3 of culture with FLAG–mFAT10 (A) and ubiquitin-encoding (B) lentiviral vectors, as well as with lentiviral vectors encoding the respective non-conjugatable forms of FLAG–mFAT10 (C) and ubiquitin (D). On day 10 of culture, immature BMDCs were stimulated (24 h) or not (0 h) using 400 U/ml TNF and 200 U/ml IFN-γ. Control BMDCs were mock-transduced and transduced with vehicle/GFP only-encoding lentiviral vectors (Fig. S1). At 4 h prior to fixation, 5 µM of MG132 was added to enrich the proteins expressed from the lentiviral vectors. Immature (0 h) and mature (24 h) BMDCs were stained for ubiquitin and FLAG-tagged proteins. Nuclei were visualised by DAPI staining and images were taken on an LSM880 confocal microscope at 63× magnification. Insets are shown to highlight colocalisation of proteins in DALIS. Representative images of three to four independent experiments are shown. Scale bars: 10 µm. (E) The insets of the merged pictures from mature BMDCs (24 h) as shown in A–D were used to create intensity profiles of endogenous ubiquitin and the respective overexpressed form of mFAT10 and ubiquitin. The intensity profiles were created along the white boxes shown in the insets. (F) Colocalisation of endogenous ubiquitin with overexpressed FAT10 or ubiquitin was quantified using the coloc2 plugin of ImageJ software, which measures the Pearson's correlation coefficient R above threshold. The box plot shows median, box (25th to 75th percentiles), and whiskers (maximum and minimum) of at least 33 DALIS in three to four independent experiments. ****P<0.0001; other values shown are not significant.

-ubiquitin from the lentiviruses was readily detectable by qPCR (Fig. S1C, left top graph and bottom graph). Of note, the level of *mFAT10* expression from the lentiviruses in KO BMDCs was twice as high as the expression level of endogenous *mFAT10* expression in WT BMDCs (Fig. S1C, right top graph and bottom graph). The transduction efficiency ranged from 40% to 60% using vehicle lentiviruses that only express GFP. Moreover, ∼20% of KO BMDCs could be transduced with FLAG–mFAT10-encoding lentiviruses, and 10–20% of WT BMDCs could be transduced with FLAG–ubiquitin-encoding lentiviruses (Fig. S1D).

Owing to initial difficulties in the detection of the lentivirally overexpressed FLAG–mFAT10 at the protein level, all immature and cytokine-matured BMDCs were incubated with the proteasome inhibitor MG132 for 4 h prior to processing for confocal microscopy to enrich the proteins expressed lentivirally. In doing so, accumulation of mFAT10 together with ubiquitin in DALIS was observed in BMDCs after 24 h of maturation (Fig. 2A, 24 h). Proteasome inhibition is known to induce the formation of aggresomes that consist of ubiquitylated, as well as FAT10ylated, proteins (Johnston et al., 1998; Kalveram et al., 2008). To exclude the possibility that a short proteasome inhibition induced aggresome formation in immature BMDCs, they were also treated with MG132 for 4 h. In immature BMDCs, neither FLAG–mFAT10 nor ubiquitin accumulated in protein aggregates, indicating that the protein aggregates observed upon BMDC maturation were DALIS and not aggresomes (Fig. 2A, 0 h). As a control, cells were transduced with a lentiviral vector that expressed FLAG–ubiquitin confirming that formation of DALIS in transduced cells was unaffected by transduction and overexpression of FLAG–mFAT10 or FLAG–ubiquitin (Fig. 2B). As observed for endogenous FAT10 in human mature MoDCs, almost all DALIS in mature BMDCs contained FLAG–mFAT10, further highlighting the targeting of murine and human FAT10 into DALIS.

Since FAT10 can be covalently attached to its substrates, it was of interest to determine whether localisation of mFAT10 into DALIS depends on conjugation. Therefore, BMDCs were transduced with a lentivirus expressing a non-conjugatable form of FLAG–mFAT10 with a mutated diglycine motif at the C-terminus (FLAG–mFAT10ΔGG). FLAG–mFAT10ΔGG accumulated in DALIS in maturing BMDCs, indicating that the localisation of mFAT10 to DALIS does not rely on conjugation and its C-terminal diglycine motif (Fig. 2C, 24 h). Interestingly, a non-conjugatable form of monomeric ubiquitin with a likewise mutated C-terminal diglycine motif (FLAG–ubiquitinΔGG) did not accumulate in DALIS (Fig. 2D, 24 h). This also excludes targeting of the overexpressed proteins to DALIS due to the relatively large 3xFLAG-6His tag and normal behaviour of the overexpressed proteins. Again, immature BMDCs were included in order to rule out unspecific aggregation of the overexpressed proteins upon proteasome inhibition by MG132 (Fig. 2C,D, 0 h).

Similar intensity profiles generated on images of cells expressing FLAG–mFAT10, FLAG–ubiquitin, and non-conjugatable FLAG–mFAT10ΔGG further confirmed specific targeting to DALIS. By contrast, the intensity profiles of endogenous ubiquitin and FLAG–ubiquitinΔGG did not correlate, indicating an exclusion from DALIS (Fig. 2E). Quantification of the colocalisation of the lentivirally overexpressed proteins with endogenous ubiquitin further substantiated our finding (Fig. 2F). Owing to the difficulties in detecting mFAT10 even after lentiviral overexpression, the number of mFAT10-positive DALIS per cell was not determined since that would have yielded data that is not statistically evaluable.

In summary, FAT10 accumulates in DALIS of human and murine mature DCs, likely through a conserved mechanism that leads to the deposition of FAT10 in essentially all DALIS that form during DC maturation. This targeting mechanism does not depend on conjugation or the C-terminal diglycine motif of mFAT10. Expression of FLAG–mFAT10 at the early stages of DC maturation neither prevented nor promoted formation of DALIS. Therefore, it can be concluded that FAT10 does not contribute to the formation of DALIS but is targeted to DALIS at later stages of DC maturation when DALIS need to be degraded.

HDAC6 is dispensable for the formation, maintenance and degradation of DALIS

FAT10 and ubiquitin are targeted to DALIS in BMDCs in a manner that is reminiscent of the targeting of both proteins to aggresomes, which requires a functional diglycine motif at the C-terminus of ubiquitin (Ouyang et al., 2012) whereas for FAT10 the diglycine motif is dispensable (Kalveram et al., 2008) (Fig. S2). Since HDAC6 is required for proper formation of aggresomes (Kawaguchi et al., 2003) and is equally important for transport of FAT10 and ubiquitin to aggresomes (Kalveram et al., 2008), these findings raised the question of whether HDAC6 might be involved in DALIS formation. To address this question, the formation of DALIS was monitored in BMDCs from WT and *HDAC6*-deficient (HDAC6 KO) mice. When HDAC6 KO and WT BMDCs were matured with cytokines, the accumulation of DALIS was equally prominent in HDAC6 KO and WT BMDCs (Fig. 3A). Likewise, the average size of DALIS was unaffected by *HDAC6* deficiency (Fig. 3B). These findings indicate that HDAC6 is not involved in DALIS formation, contrary to aggresomes where HDAC6 is necessary for proper formation (Kawaguchi et al., 2003). The similar maturation and phenotype of the HDAC6 KO and WT BMDCs were confirmed by measuring surface expression levels of CD11c, CD86 and MHC class II, and by determining *mFAT10* expression levels upon maturation (Fig. S3A,B). Additionally, *mHDAC6* was highly expressed at a constant level in maturing BMDCs (Fig. S3B), and HDAC6 KO and WT BMDCs were equally viable (Fig. S3C). Additionally, we treated mature and immature WT BMDCs with the proteasome inhibitor MG132 alone or in combination with nocodazole to test whether BMDCs are generally able to form

Journal of Cell Science (2020) 133, jcs240085. doi:10.1242/jcs.240085

aggresomes. Nocodazole depolymerises microtubules and, as such, has been used to prevent the formation of aggresomes, which depends on a functioning microtubule network (Johnston et al., 1998; Kalveram et al., 2008). Interestingly, in BMDCs treated with MG132, we observed cells that contained only DALIS, only aggresomes, or DALIS and aggresomes together (Fig. 3C). Enumeration of cells that had formed DALIS and aggresomes (Fig. 3D) showed that DALIS formation in BMDCs was not substantially affected upon induction of aggresomes, as the number of DALIS did not change significantly in immature and mature cells treated with MG132 alone or MG132 and nocodazole together (Fig. 3D, left graph). Furthermore, the formation of aggresomes was not affected by maturation of BMDCs (Fig. 3D, middle graph), since we found the same percentage of cells showing aggresomes after treatment with MG132 in immature and mature BMDCs. BMDCs treated with MG132 and nocodazole showed almost no aggresome formation (Fig. 3D, middle graph), but still contained DALIS (Fig. 3D, left graph) confirming that aggresome formation is dependent on a functioning microtubule network whereas DALIS formation is not (Lelouard et al., 2004). Although the percentage of BMDCs that formed both DALIS and aggresomes (Fig. 3D, right graph) was lower than the percentage of total cells showing either DALIS or aggresomes (Fig. 3D, left and middle graph), BMDCs nevertheless were able to form aggresomes and DALIS simultaneously in the same cell. Taken together, these results indicate that HDAC6 is not involved in the formation, maintenance and disassembly of DALIS, a trait that further distinguishes DALIS from aggresomes.

FAT10 contributes to the disassembly of DALIS

To investigate whether the lack of mFAT10 has an influence on DALIS, we generated BMDCs from FAT10-deficient (KO BMDCs) and -proficient (WT BMDCs) mice. First, the maturation of KO and WT BMDCs induced by LPS and by the pro-inflammatory cytokines TNF and IFN-γ was compared. DALIS were visualised by staining for p62 and ubiquitin, which both have been reported to localise to DALIS in mature BMDCs (Lelouard et al., 2002; Terawaki et al., 2015). The maturation and phenotype of KO and WT BMDCs were determined by measuring surface levels of CD11c, CD86 and MHC class II, and determining *mFAT10* expression levels upon maturation (Fig. S4C). Microscopy imaging revealed no obvious morphological differences upon stimulation between KO and WT BMDCs that were matured through LPS (data not shown) or cytokines (Fig. 4A). Both KO and WT BMDCs formed DALIS that stained positive for ubiquitin and p62 during a time course of 48 h upon maturation with LPS or cytokines (Fig. 4A, highlighted by insets). Owing to the lack of an antibody for detection of mFAT10 at the protein level, the expression of mFAT10 after maturation was quantitatively determined at the mRNA level. We found expression of mFAT10 after 8 h of induction until 48 h, with higher expression levels upon induction with cytokines as compared to LPS induction (Fig. 4B). Additionally, we quantified how many BMDCs formed DALIS in an immature state, which we consider spontaneous maturation, and after 24 h of maturation by cytokines (Fig. 4C). We observed that 30% of immature BMDCs already showed DALIS, which increased to 80% of cells showing DALIS after 24 h of maturation by cytokines. Expression of the mFAT10 conjugation machinery (i.e. *USE1* and *UBA6*), was not considerably up- or down-regulated during BMDC maturation using the different maturation stimuli. Likewise, there was no differential regulation of *UBA6* and *USE1* between KO and WT BMDCs (Fig. S4A). Since expression of *UBA6* and *USE1* does not change during DC maturation and since it has been reported that protein translation decreases during DC maturation (Argüello et al., 2016; Ceppi et al., 2009; Lelouard et al., 2007) these results suggest that conjugation of FAT10 is not enhanced but rather decreases during BMDC maturation. Taken together these results suggest that mFAT10 and its conjugation are not essential for DALIS formation although mFAT10 is present at times when DALIS formed.

Several studies have reported that DALIS form transiently in DCs peaking between 8 and 12 h of LPS stimulation (Canadien et al., 2005; DeFillipo et al., 2004; Herter et al., 2005; Kettern et al., 2011; Lelouard et al., 2002; Faßbender et al., 2008). We determined the number of DALIS from images as shown in Fig. 4A in cytokine- and LPS-matured KO and WT BMDCs. In LPS-stimulated BMDCs, DALIS started to accumulate noticeably after 8 h, increased minimally at 24 h, and decreased at 48 h (Fig. 4D, right panel). Although DALIS formation did not peak at 8 h after LPS stimulation, these results are globally consistent with the reported kinetics for DALIS formation, since the peak of DALIS formation could have been missed if it was between 8 and 24 h. Interestingly, the kinetics of DALIS formation upon cytokine stimulation differed from the kinetics observed in previous reports in that the number of DALIS in FAT10 KO and WT BMDCs increased strongly after 24 h and then decreased slightly at 48 h of maturation suggesting delayed kinetics in these cells (Fig. 4D, left panel). We observed similar kinetics when comparing HDAC6 KO to WT BMDCs (Fig. 3A). Likewise, delayed kinetics of ALIS formation has been reported in IFN-γ-treated mouse embryonic fibroblasts (Nathan et al., 2013), suggesting that the observed delay is likely due to the cytokine stimulation used for inducing maturation and DALIS formation. When comparing DALIS formation in WT and KO BMDCs at the single time points, no differences were found when BMDCs were matured with LPS. However, significantly less DALIS were detected in WT compared to FAT10-deficient BMDCs at 24 h and also less at 48 h of maturation suggesting that FAT10 participated in clearance of DALIS at these time points. These findings are underscored by the level of *FAT10* expression in these cells (Fig. 4B), where high expression of *FAT10* mRNA was found after cytokine stimulation and low levels of *FAT10* transcripts after maturation with LPS. This might also explain why there was no FAT10-mediated effect on the kinetics of DALIS in LPS-matured BMDCs. The size of the DALIS did not differ between KO and WT BMDCs at any time point during maturation (Fig. 4E) and also not after cycloheximide treatment (data not shown), suggesting that FAT10 neither specifically targets proteins within DALIS for degradation nor enhances the formation of larger aggregates. Thus, FAT10 leads to the rapid removal of entire DALIS as observed by the decreased number. Experiments were performed to confirm these results by means of immunoblotting of detergent-insoluble fractions, which contain DALIS, and detergent-soluble fractions, which do not, as has been reported by Lelouard and colleagues (Lelouard et al., 2002). However, DALIS fractions could not be reproducibly isolated despite testing two different published protocols (Lelouard et al., 2002; Rahnefeld et al., 2011) and one group-internal protocol.

Up-regulation of *p62* in LPS-stimulated macrophages is crucial for the formation of ALIS (Fujita et al., 2011), and *p62* is induced upon cytokine treatment in HEK293 cells (Aichem et al., 2012). Therefore, we investigated p62 expression at the protein and mRNA level in cytokine- or LPS-matured BMDCs (Fig. S4A). We did not observe any difference of *p62* expression between KO and WT BMDCs. However, *p62* levels increased by 2-fold in cytokine-matured BMDCs, which is not as high as reported by Aichem and

Journal of Cell Science (2020) 133, jcs240085. doi:10.1242/jcs.240085

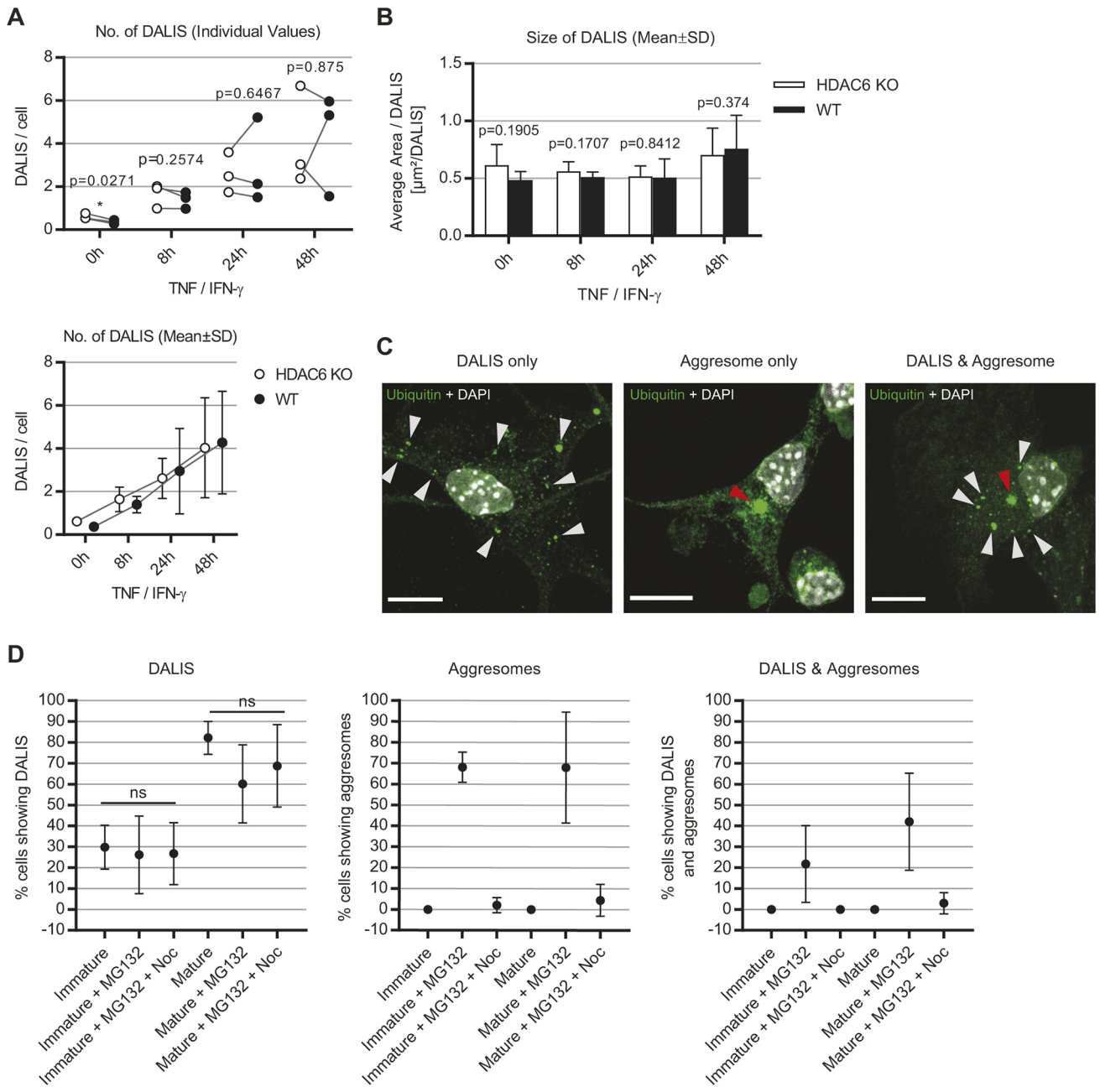

Fig. 3. Comparison of DALIS and aggresome formation in *HDAC6*-deficient and -proficient DCs. *HDAC6*-deficient (HDAC6 KO) and -proficient (WT) BMDCs were generated and maturation was induced using 400 U/ml TNF and 200 U/ml IFN-γ. At the indicated time points, BMDCs were analysed by confocal microscopy. BMDCs were stained for ubiquitin, and the number of DALIS and aggresomes as well as the area of DALIS was determined using ImageJ software. (A) The average number of DALIS per cell is depicted using a before-and-after graph (left graph) and is shown as the mean±s.d. (right graph). Lines connect individual data points from the same experiments at the indicated time points. (B) The total area of ubiquitin-positive DALIS was normalised to the number of DALIS and is given as the mean±s.d. In A and B, results are from three independent experiments, where each data point (open and filled circles) represents the mean of at least 64 analysed cells. The data was analysed statistically using two-tailed paired *t*-tests comparing HDAC6 KO and WT at the individual time points. *P*-values are indicated above the respective comparison [*P<0.05; other values shown are not significant]. (C) Representative images of 24 h-matured, HDAC6-proficient BMDCs treated with MG132 for 6 h to induce aggresome formation showing only DALIS (left), only aggresomes (middle), or DALIS and aggresomes at the same time (right). DALIS and aggresomes were visualised by ubiquitin staining (green), and nuclei by DAPI staining (grey). The ubiquitin and DAPI staining are both shown in the merge in the images. DALIS are highlighted by white arrowheads and aggresomes by red arrowheads. Scale bars: 10 µm. (D) Quantification of percentage of cells showing DALIS, aggresomes and both in immature and 24 h-matured BMDCs. BMDCs were left untreated, treated with 5 µM MG132 for 6 h to induce aggresome formation, and treated with a combination of 5 µM MG132 and 1 µM nocodazole for 6 h to prevent aggresome formation. Data points represent the mean±s.d. of three independent experiments where at least 21 cells were analysed per experiment; ns, not significant.

colleagues in HEK293 cells, but can be accounted for by the different cell types used. Maturation of BMDCs induced by LPS increased *p62* mRNA levels by 3–5-fold, which is in line with the report of Fujita and colleagues (Fujita et al., 2011). At the protein level, we found a stimulus-dependent increase of p62 (Fig. S4B) that almost reflects the kinetics of DALIS formation

Journal of Cell Science (2020) 133, jcs240085. doi:10.1242/jcs.240085

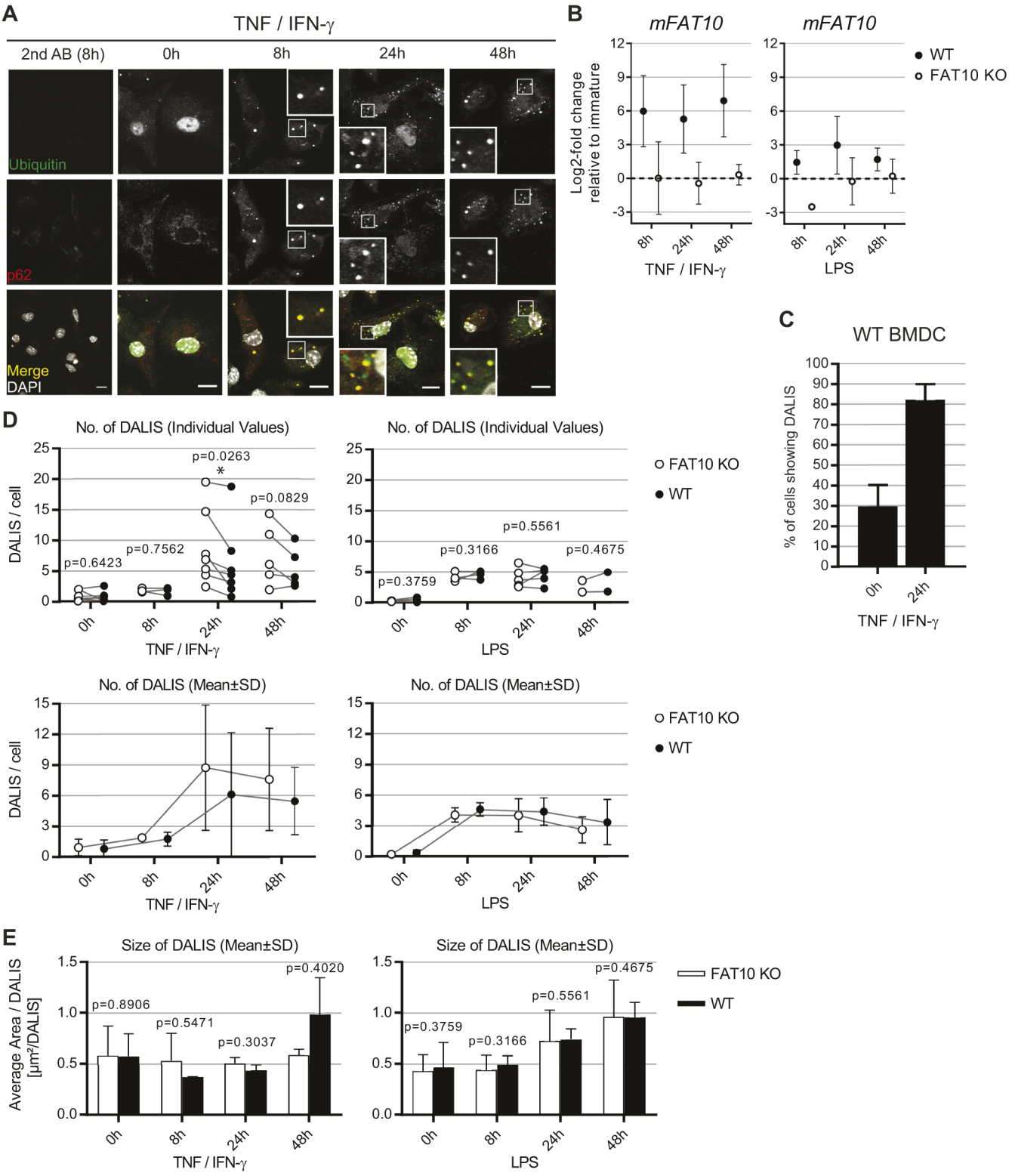

Fig. 4. See next page for legend.

and disassembly that we observed in our microscopy-based analysis (Fig. 4D). We also did not observe a direct correlation between the *p62* mRNA levels with p62 protein levels in BMDCs, in contrast to what has been observed in HEK293 cells upon cytokine stimulation suggesting an additional level of post-transcriptional regulation in DCs as compared to HEK293 cells (Aichem et al., 2012). In summary, we found an increase of p62 protein upon BMDC maturation, which points at a decreasing level of autophagy (Bjørkøy et al., 2005), that allows for the efficient DALIS formation in our BMDC preparations. This is in line with previous studies where a decrease of autophagy was found to be necessary for efficient

Journal of Cell Science (2020) 133, jcs240085. doi:10.1242/jcs.240085

Fig. 4. DALIS accumulation in DCs upon cytokine and LPS stimulation. *FAT10*-deficient (KO) and -proficient (WT) BMDCs were matured with 400 U/ml TNF and 200 U/ml IFN-γ or 1 µg/ml LPS. (A) Cytokine-matured BMDCs were stained with anti-p62 and anti-ubiquitin antibodies or secondary antibodies only [2nd AB (8 h)], and analysed by confocal microscopy. Nuclei were counterstained with DAPI. Representative images of three to seven independent experiments are shown and insets are included to highlight colocalisation. Images show FAT10-deficient BMDCs, except at 48 h where FAT10-proficient BMDCs are displayed. Scale bars: 10 µm. (B) Expression levels of *mFAT10* were determined by qPCR in cytokine- and LPS-induced BMDCs. Expression levels were normalised to *mHPRT* and depicted as log2-fold change relative to immature KO or WT BMDCs (indicated as dotted line). Results of two to six experiments are shown. (C) The percentage of cells showing DALIS is depicted for FAT10-proficient BMDCs matured with cytokines for the indicated time points. Three independent experiments, where at least 30 cells were analysed per experiment, are summarised and depicted as mean±s.d. The data has been extracted from the results shown in the left graph in Fig. 3D. (D,E) At the indicated time points KO and WT BMDCs were stained for ubiquitin following the quantification of the number (D) and the area (E) of DALIS of at least 50 cells per experiment using ImageJ software. (D) The average number of DALIS per cell per performed experiment is depicted using a before-and-after graph (upper panel) and is shown as the mean±s.d. (lower panel). Lines connect individual data points from the same experiments at the indicated time points. Results are shown for three to seven experiments for cytokine induction and two to five experiments for LPS induction. (E) The total area of ubiquitin-positive DALIS was normalised to the number of DALIS and graphed as mean±s.d. The area of DALIS was determined from two to three experiments of cytokine-matured BMDCs and from two to five experiments of LPS-matured BMDCs. Statistical significance was calculated by two-tailed paired *t* tests at the individual time points. *P*-values are indicated above the respective comparison [**P*<0.05; other values shown are not significant].

ALIS formation in HeLa cells and macrophages (Terawaki et al., 2015; Wenger et al., 2012).

Next, the effect of FAT10 observed at 24 h of maturation was further examined. The cytokine-matured KO and WT BMDCs were incubated with cycloheximide 2 h prior to fixation and staining for confocal microscopy in order to inhibit protein neosynthesis. Thereby FAT10-mediated degradation of DALIS can be detected through a microscopy approach that is similar to cycloheximide chase experiments followed by immunoblotting. Since mFAT10 has a half-life of ∼1 h (Hipp et al., 2005; Raasi et al., 2001), we expected to see FAT10-mediated resolution of DALIS after 2 h of cycloheximide treatment. It can be excluded that the cycloheximide treatment influenced the formation of DALIS at 24 h since protein synthesis was shown to be only important at early stages of DALIS formation (Lelouard et al., 2002). After determining the number of DALIS per cell in cycloheximide-treated mature BMDCs (Fig. 5A), a significant increase of DALIS numbers in the KO BMDCs compared to untreated KO BMDCs was evident, whereas cycloheximide treatment had no effect on the number of DALIS in WT BMDCs. The sudden increase of ubiquitylated proteins in cycloheximide-treated KO BMDCs was probably caused by increased targeting of long-lived proteins into the aggregates. A similar effect of cycloheximide on ALIS has been observed in mouse embryonic fibroblasts under starvation conditions (Szeto et al., 2006) and in INS1 832/13 β-cells under normal and high-glucose conditions (Kaniuk et al., 2007). Since there was no accumulation in WT BMDCs, it can be concluded that FAT10 counteracted the increased flux of long-lived proteins into DALIS through proteasomal degradation, which has been shown before for FAT10 fusion proteins (Ebstein et al., 2012; Schliehe et al., 2012) as well as FAT10 substrates (Aichem et al., 2010; Bialas et al., 2015).

In addition, a possible contribution of endogenous FAT10 to the formation of DALIS and to the targeting of DALIS into the autophagolysosomal pathway was investigated. To this aim, autophagy initiation was inhibited using wortmannin (Fig. 5B) and the proteasome was inhibited using MG132 (Fig. 5C). The number of DALIS in KO and WT mature BMDCs increased equally upon inhibition of autophagy compared to untreated cells (Fig. 5B), suggesting that FAT10 does not substantially target DALIS into the autophagolysosomal degradation pathway and that autophagy inhibition does not enhance FAT10-mediated degradation of DALIS by the proteasome. The observed increase of DALIS, however, indicated bulk turnover of DALIS by autophagy in BMDCs matured by cytokines, which is in line with previous findings where increased ALIS formation was observed in macrophages and HeLa cells after inhibition of autophagy (Szeto et al., 2006). However, this result is in contrast to the proposed degradation mechanisms after LPS stimulation, which suggests that reduced autophagy leads to enhanced proteasomal degradation of DALIS (Argüello et al., 2016). There was no FAT10-specific accumulation of DALIS when the proteasome was inhibited (Fig. 5C), confirming that endogenous FAT10 does not contribute to the formation of DALIS as observed after homologous overexpression of FLAG–mFAT10 (Fig. 2).

To confirm the FAT10-mediated effects observed after cycloheximide treatment of BMDCs, we lentivirally re-expressed FLAG–mFAT10 in FAT10-deficient BMDCs followed by cycloheximide treatment (Fig. 5D). Transduction was controlled by flow cytometry detecting GFP, which was co-expressed from the same lentiviral constructs as FLAG-mFAT10, and we achieved 44.2±12.24% transduced cells (mean±s.d., data not shown). The number of DALIS in untreated WT and KO BMDCs, as well as transduced KO BMDCs did not differ. Upon treatment of the BMDCs with cycloheximide, the number of DALIS in KO BMDCs increased as observed above (Fig. 5A). This increase was not observable in BMDCs that had been transduced with FLAG–mFAT10. This suggests that FAT10 was able to counteract the increased flux of long-lived proteins into DALIS, very likely by proteasomal degradation.

DISCUSSION

FAT10 expression is upregulated upon DC maturation (Ebstein et al., 2009; Lukasiak et al., 2008), and has been linked to antigen processing and presentation (Basler et al., 2015; Ebstein et al., 2012; Schliehe et al., 2012). Furthermore, FAT10 localises to aggresomes in a largely HDAC6-dependent manner and with its interaction partner p62/sequestosome 1 into p62 bodies in HeLa cells (Aichem et al., 2012; Kalveram et al., 2008). Based on these findings we investigated whether FAT10 also localises to DALIS and is involved in DALIS regulation. We found that both endogenous human FAT10 and overexpressed murine FAT10 localised to DALIS. Interestingly we observed that all DALIS contain human or murine FAT10, indicating a specific function of FAT10 in the regulation of DALIS in human as well as murine DCs. Targeting to DALIS did not depend on the diglycine motif of FAT10 strongly arguing against a need for conjugation. Therefore, it can be assumed that FAT10 conjugation takes place within DALIS, similar to the conjugation of ubiquitin that can occur within DALIS as indicated by the presence of the ubiquitin conjugation machinery in DALIS, such as the E1 enzyme UBE1 and the E3 ligase CHIP (Kettern et al., 2011; Lelouard et al., 2004). However, we do not know whether the FAT10 conjugation enzymes UBA6 and USE1 also localise to DALIS.

Kalveram et al. previously reported that delivery of FAT10 to aggresomes relies on HDAC6, which interacts with both ubiquitin-like domains of FAT10 (Kalveram et al., 2008). Here, we have shown that HDAC6 is dispensable for the formation and clearance

Journal of Cell Science (2020) 133, jcs240085. doi:10.1242/jcs.240085

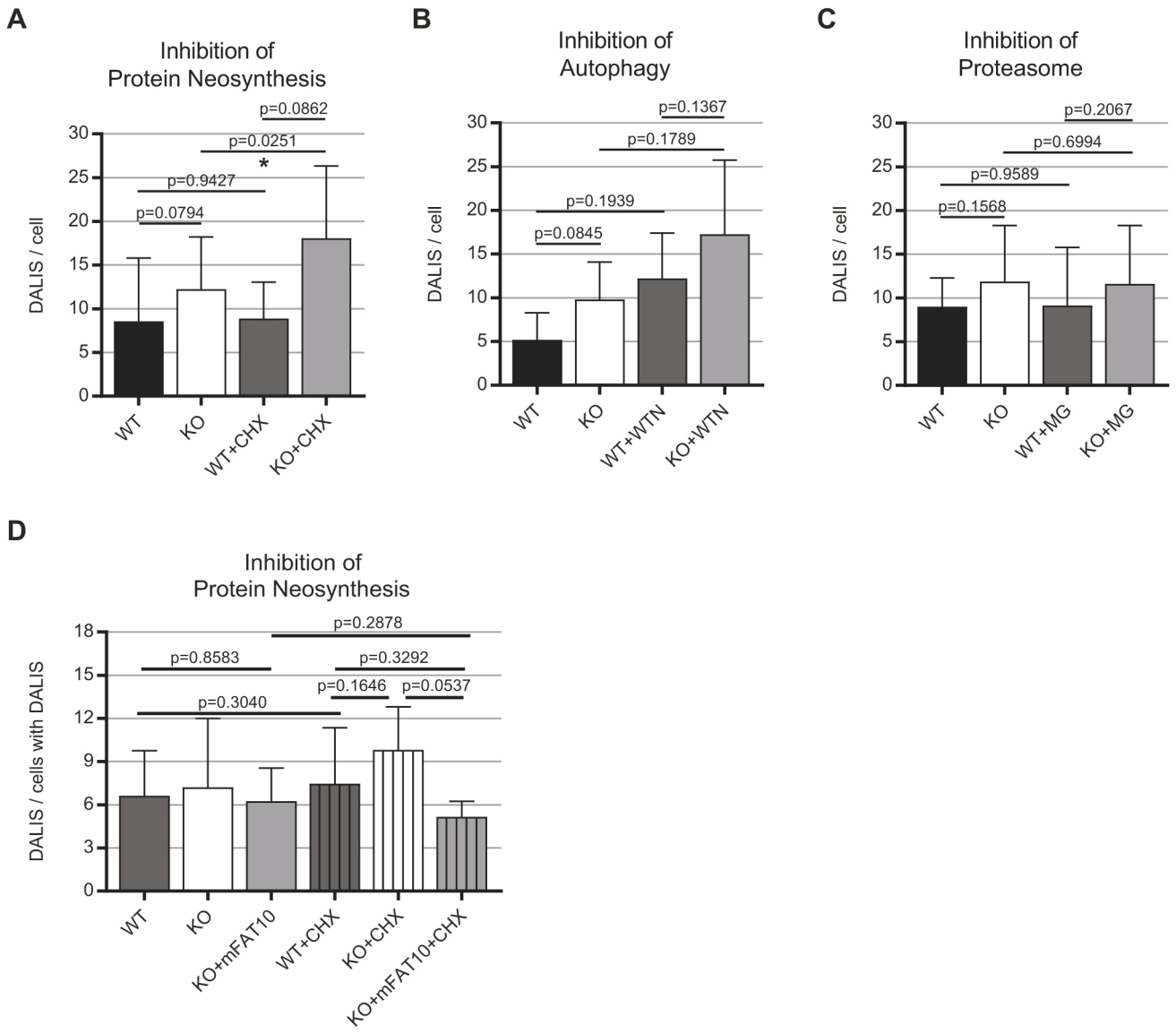

Fig. 5. Influence of inhibition of protein synthesis and degradation on DALIS disassembly in *FAT10*-deficient and -proficient mature BMDCs. *FAT10*-deficient (KO), FAT10-proficient (WT), and *FAT10*-deficient BMDCs lentivirally re-constituted with mFAT10 (KO+mFAT10) were induced using 400 U/ml TNF and 200 U/ml IFN-γ for 24 h. At 2 h prior to fixation and ubiquitin staining 10 µg/ml cycloheximide (CHX) (A,D), 2 µM wortmannin (WTN) (B) and 10 µM MG132 (MG) was added (C). Enumeration of ubiquitin-positive DALIS from three to four experiments is shown. At least 50 cells per experiment were analysed. The different inhibitor treatments were partially performed simultaneously within one experiment and therefore the results from untreated KO and WT BMDCs overlap within the different graphs. DALIS per cell are plotted as mean±s.d. for indicated samples except in D, where DALIS are normalised to the number of cells showing DALIS and are plotted as mean±s.d. Statistical significance was calculated by RM one-way ANOVA following the indicated planned comparisons using uncorrected Fisher's LSD test. *P*-values are indicated above the respective planned comparison [**P*<0.05; other values shown are not significant].

of DALIS since *HDAC6*-deficient murine BMDCs showed no difference in the kinetics of DALIS formation compared to *HDAC6*-proficient BMDCs. Hence, it appears that FAT10 is targeted to DALIS in DCs by another mechanism. DALIS are motile within the cytosol and can undergo fusion suggesting that this motility is necessary for the aggregation process (Lelouard et al., 2004). This movement also occurs along microtubules since nocodazole treatment instantly abrogates DALIS motility (supplementary video 2 in Canadien et al., 2005). Based on our observation that DALIS and aggresomes can occur in the same cell (Fig. 3C,D), we consider it unlikely that movement of DALIS along microtubules occurs via HDAC6 since then we would expect smaller and more aggregates in *HDAC6*-deficient cells, which was not the case. Additionally, if HDAC6 was necessary for the motility of DALIS, we would expect that DALIS would eventually end up in the aggresome at the MTOC, which they did not. This further argues against a role of HDAC6 in this process and in the targeting of FAT10 to DALIS. Theoretically, spartin, a protein that is involved in cytokinesis and mitochondrial physiology (Joshi and Bakowska, 2011; Renvoisé et al., 2010), could be responsible for DALIS motility. Spartin is partially necessary for the formation of DALIS since knockdown of Spartin in RAW264.7 macrophages reduced the formation of DALIS (Karlsson et al., 2014). Additionally, Spartin contains a 'microtubule interacting and trafficking' motif with which it can bind to microtubules (Lu et al., 2006). However, this hypothesis needs further investigation.

Next, we compared the formation of DALIS in *FAT10*-deficient and -proficient BMDCs upon maturation with LPS or cytokines

Journal of Cell Science (2020) 133, jcs240085. doi:10.1242/jcs.240085

(TNF and IFN-γ). LPS-matured BMDCs formed DALIS as expected and reported previously (Canadien et al., 2005; DeFillipo et al., 2004; Herter et al., 2005; Kettern et al., 2011; Lelouard et al., 2002). By contrast, the kinetics of the cytokine-induced DALIS formation differed from previous reports and showed a delay in accumulation that first was apparent at 24 h, with no substantial increase at 8 h. This kinetics is similar to the IFN-γ-induced formation of ALIS in murine embryonic fibroblast observed by Nathan and colleagues who found an increase of the number of ALIS up to 48 h (Nathan et al., 2013), but, stands in contrast to the results by Seifert and colleagues who reported the canonical ALIS kinetics, with an increase up to 8 h and a subsequent decrease of the number of ALIS (Seifert et al., 2010). Thus, the discrepancy between the LPS- and cytokine-induced DALIS kinetics we observed is very likely not due to different maturation stimuli. Furthermore, we can exclude that this difference is dependent on *FAT10* expression since we observed the same kinetics in *FAT10*-deficient and -proficient cells. To date we have no explanation for the different DALIS kinetics in cytokine- and LPS-matured BMDCs.

At later stages of DC maturation, the numbers of DALIS in *FAT10*-proficient BMDCs was reduced compared to *FAT10*-deficient BMDCs suggesting that FAT10 contributed to the degradation of DALIS. Since proteasomes do not localise to DALIS (Canadien et al., 2005; Herter et al., 2005), the transport of FAT10 and FAT10ylated substrates to proteasomes could be mediated by UBL-UBA domain proteins, such as NUB1L and ubiquilins. These proteins serve as soluble ubiquitin receptors and deliver their clients, such as FAT10, to the proteasome enabling degradation according to the proposed 'transfer model' of FAT10 degradation (Rani et al., 2012). The overall effect of FAT10 on the degradation of DALIS was small considering that FAT10 is present in almost all DALIS as evident from our colocalisation studies in human and murine DCs. This suggests that most of the FAT10 that is present in DALIS is not conjugated, which is in line with the general observation that most of the cellular FAT10 is present in its monomeric form, despite its conjugation to hundreds of substrates (Aichem et al., 2012). Additionally, conjugation of FAT10 to newly synthesised proteins or puromycin-induced DRiPs, which are the main constituent of DALIS (Lelouard et al., 2002; Lelouard et al., 2004), occurs at a lower rate than, for example, conjugation of ISG15 and ubiquitin, further supporting our finding (Spinnenhirn et al., 2017). To confirm that the reduced number of DALIS in *FAT10*-proficient BMDCs at 24 h was due to degradation of DALIS mediated via FAT10, we utilised a cycloheximide chase approach in combination with microscopy quantification of DALIS. After applying cycloheximide for 2 h, we observed increased numbers of DALIS in *FAT10*-deficient BMDCs, whereas the number of DALIS in *FAT10*-proficient BMDCs and in FAT10-deficient BMDCs with re-constituted FLAG–mFAT10 remained unchanged. Although this confirmed FAT10-mediated clearance of DALIS, this effect was surprising since we expected a decrease of DALIS at 24 h of maturation. At this time point, the formation of DALIS should have ceased and clearance should take place as has been reported previously (Canadien et al., 2005; Herter et al., 2005; Kettern et al., 2011; Lelouard et al., 2002). However, an increase of ALIS after cycloheximide treatment has been reported in INS1 832/13 β-cells under normal and high-glucose conditions (Kaniuk et al., 2007). The same group reported that ALIS formation in mouse embryonic fibroblasts under starvation conditions was only partially inhibited by cycloheximide treatment at an early stage of ALIS formation (Szeto et al., 2006), which should be dependent on protein synthesis (Lelouard et al., 2002). Both studies concluded that this was the result of an influx of long-lived proteins into DALIS. Relating these data to our experiments, we conclude that FAT10 counteracted the influx of long-lived proteins by promoting their efficient proteasomal degradation. This FAT10-mediated flux of proteins or antigens from DALIS into the proteasome argues in favour of an involvement of FAT10 in antigen processing and presentation via the MHC class I presentation pathway. To address this issue in more detail, it would be necessary to elucidate the targets of FAT10 within DALIS. In theory, FAT10 could target pathogenic proteins that accumulate in DALIS for proteasomal degradation and thereby enhance MHC class I presentation of these antigens. In support of this hypothesis, fusion of FAT10 to long-lived viral proteins accelerated their degradation and enhanced the subsequent presentation on MHC class I (Ebstein et al., 2012; Schliehe et al., 2012), and the overexpression of FAT10 changes the spectrum of peptides presented on MHC class I (Buerger et al., 2015). Besides that, accumulation of viral proteins in DALIS in DCs has been observed (Herter et al., 2005; Rahnefeld et al., 2011). In the case of the influenza nucleoprotein (NP) it has been shown that the retention of NP in DALIS in BMDCs delayed antigen presentation, and that antigen presentation increased concurrently with upregulation of co-stimulatory molecules and MHC class I molecules on the surface of BMDCs in order to more efficiently prime T cells (Herter et al., 2005). Yet, conjugation of endogenous FAT10 to pathogen-derived proteins or antigens still awaits discovery.

Furthermore, we did not see FAT10-specific formation of DALIS in BMDCs since the number of DALIS did not change in a FAT10-specific manner upon proteasome inhibition. Likewise, overexpression of 3xFLAG–mFAT10 in BMDCs did not interfere with DALIS formation. This can be explained by the short half-life of FAT10 of ∼1 h (Aichem et al., 2014; Hipp et al., 2005; Raasi et al., 2001; Schmidtke et al., 2014) and the high turnover that was evident in our experiments where we only detected overexpressed 3xFLAG–mFAT10 in BMDCs upon proteasome inhibition, given that FAT10 is mostly present in its non-conjugated monomeric form and not preferentially conjugated to DRiPs (Spinnenhirn et al., 2017) that are stored in DALIS. Interestingly, inhibition of autophagy using wortmannin increased the number of DALIS in *FAT10*-deficient and -proficient BMDCs indicating that DALIS are targeted substantially into the autophagolysosomal pathway and that targeting into autophagy occurs independently of FAT10. These results are in line with former findings where FAT10-mediated targeting into autophagy was not detected (Spinnenhirn, 2014). However, FAT10 has been shown to positively influence targeting of cytosolic *Salmonella* bacteria for autophagy (Spinnenhirn et al., 2014), and covalently as well as non-covalently binds to p62 (Aichem et al., 2012). Thus, specific pathogenic antigens, which were not present in this study, may be targeted by FAT10 from DALIS into autophagy by interacting with p62 in DALIS and thereby FAT10 could feed antigens into the MHC class II presentation pathway. In summary, the cardinal findings of this study are that FAT10 localises to DALIS, does not contribute to DALIS accumulation, and can feed antigens from DALIS into the proteasome and thereby might contribute to antigen presentation and to shape the pool of peptides presented on MHC class I molecules.

MATERIALS AND METHODS

Mice

C57BL/6 (H-2^b) mice were originally purchased from Charles River Laboratories (Sulzfeld, Germany). Allon Canaan and Sherman M. Weissman (Yale University School of Medicine, New Haven, CT,

Journal of Cell Science (2020) 133, jcs240085. doi:10.1242/jcs.240085

USA) kindly provided *FAT10*-deficient mice (Canaan et al., 2006). Mice were housed in a specific pathogen-free facility. For experiments, we used sex- and age-matched mice at 8–12 weeks of age. Hind legs of *HDAC6*-deficient mice (Zhang et al., 2008) and corresponding sex- and age-matched wild-type C57BL/6 mice were kindly provided by Patrick Matthias (Friedrich Miescher Institute for Biomedical Research, Basel, Switzerland). Isolation of primary cells from mice was performed in accordance with the German Animal Welfare Act and approved by the animal welfare officer of the University of Konstanz or, if applicable, by the review board of the Regierungspräsidium Freiburg.

Cell culture

Human embryonic kidney (HEK) 293T cells were cultured in Iscove's Modified Dulbecco's Medium (IMDM) supplemented with 10% heat-inactivated fetal calf serum (iFCS), 100 U/ml penicillin and 100 µg/ml streptomycin. Primary mouse cells were cultured in Roswell Park Memorial Institute 1640 (RPMI 1640) medium supplemented with 10% iFCS, 50 µM β-mercaptoethanol, 100 U/ml penicillin and 100 µg/ml streptomycin (complete RPMI 1640). Primary human cells were cultured in AIM-V supplemented with 2% heat-inactivated human AB serum (Sigma-Aldrich, Munich, Germany) and 50 µM β-mercaptoethanol (complete AIM-V). Primary human cells were isolated from peripheral human blood from healthy donors. The ethics committee of the University of Konstanz approved blood donations for research purposes, and individual donors gave written consent. Cell culture media contained the GlutaMAX™ supplement. Unless otherwise stated all media and supplements were purchased from Thermo Fisher Scientific (Schwerte, Germany). Cell lines were regularly checked to be free of mycoplasma or other contaminations.

Generation of bone-marrow derived dendritic cells

Bone marrow-derived dendritic cells (BMDCs) from *HDAC6*-deficient, *FAT10*-deficient and wild-type C57BL/6 mice were generated as described previously (Lutz et al., 1999). Briefly, we rinsed the bone marrow from femurs and tibiae and washed the cells with PBS. Contaminating erythrocytes were lysed in ACK buffer (8.29 g/l NH_4Cl, 1 g/l $KHCO_3$, 0.1 mM EDTA; all from Carl Roth, Karlsruhe, Germany) for 5 min at room temperature (RT) and subsequently washed with PBS supplemented with 5 mM EDTA. Finally, we seeded the bone marrow cells at 2×10^5 cells/ml into bacteriological 10 cm Petri dishes (Carl Roth, Karlsruhe, Germany) (day 0) in 10 ml of complete RPMI 1640 additionally supplemented with 200 U/ml murine granulocyte/macrophage-colony stimulating factor (GM-CSF; PeproTech, Hamburg, Germany). On day 3 of culture, 10 ml of fresh complete RPMI 1640 were added. On days 6 and 8 of culture, half of the culture medium was removed, non-adherent cells pelleted, resuspended in fresh complete RPMI 1640, and 10 ml per Petri dish transferred back to the original culture dishes. Fully differentiated immature BMDCs were obtained on day 9 or 10.

Generation of monocyte-derived dendritic cells

We generated monocyte-derived DCs (MoDCs) from human $CD14^+$ monocytes. Monocytes were isolated by magnetic cell sorting (MACS) from peripheral human blood from healthy donors. First, peripheral blood mononuclear cells (PBMCs) were enriched by density gradient centrifugation using Ficoll-Paque Plus (GE Healthcare, Freiburg, Germany) and washed several times with PBS supplemented with 0.5% heat-inactivated human AB serum and 2 mM EDTA (MACS buffer) to remove as many platelets as possible. We removed remaining erythrocytes by lysis in ACK buffer and incubation for 5 min at RT. After a final washing step with MACS buffer, PBMCs were subjected to MACS and the $CD14^+$ monocytes enriched using anti-CD14-conjugated microbeads (Miltenyi Biotec, Bergisch Gladbach, Germany) according to the manufacturer's instructions. Purified monocytes were cultured at 2×10^6 cells/ml in complete AIM-V medium additionally supplemented with 500 U/ml human GM-CSF and 250 U/ml human interleukin-4 (IL-4) (both from PeproTech, Hamburg, Germany). On the next day (day 1), the same volume of complete AIM-V medium containing 500 U/ml human GM-CSF and 250 U/ml human IL-4 was added. On day 6 of culture, monocytes were fully differentiated into immature MoDCs and used for experiments.

Dendritic cell maturation and drug treatment

To induce maturation of DCs we added either lipopolysaccharide (LPS; Sigma-Aldrich, Munich, Germany) or a cytokine cocktail to the culture medium. We used LPS at a final concentration of 1 µg/ml together with 200 U/ml murine GM-CSF for BMDCs, or in combination with 500 U/ml human GM-CSF and 250 U/ml human IL-4 for MoDCs. For human MoDCs a cytokine cocktail consisting of 500 U/ml human GM-CSF, 250 U/ml human IL-4, 200 U/ml human interleukin-6 (IL-6), 10,000 U/ml human interleukin-1β (IL-1β), 400 U/ml human tumour necrosis factor (TNF) and 200 U/ml human interferon-γ (IFN-γ) was used to induce maturation. Maturation of BMDCs was induced using a cytokine cocktail containing 200 U/ml murine GM-CSF, 400 U/ml murine TNF, and 200 U/ml murine IFN-γ. In some experiments, BMDCs were treated with 10 µM MG132 (Enzo Life Sciences, Lörrach, Germany), 10 µg/ml cycloheximide (CHX; Sigma-Aldrich, Munich, Germany) and 2 µM wortmannin (WTN; Sigma-Aldrich, Munich, Germany) for 2 h before fixation and immunostaining. Transduced BMDCs were treated with 5 µM MG132 for 4 h prior to processing for confocal microscopy. To induce aggresome formation, BMDCs were treated with 5 µM MG132 (Enzo Life Sciences, Lörrach, Germany) for 6 h prior to fixation. Where indicated, aggresome formation of MG132-treated BMDCs was prevented by treatment with 1 µM nocodazole (Noc; Sigma-Aldrich, Munich, Germany). All cytokines were purchased from PeproTech (Hamburg, Germany).

Lentiviral vector constructs

The cDNAs of human *FAT10* (hFAT10) and murine *FAT10* (mFAT10) as well as the respective non-conjugatable forms of human *FAT10* (hFAT10ΔGG) and murine *FAT10* (mFAT10ΔGG) were PCR-amplified and inserted into the *Nhe*I and *Not*I sites of the HIV-based lentiviral plasmid vector pCDH-CMV-MCS-EF1α-copGFP (BioCat, Heidelberg, Germany). The cDNA of wild-type ubiquitin (Ub) and non-conjugatable ubiquitin (UbΔGG) was PCR-amplified and inserted into the *Eco*RI and *Not*I sites of the HIV-based lentiviral plasmid vector pCDH-EF1α-hFAT10-IRES-copGFP (Schmidtke et al., 2017). All cDNAs were expressed with an N-terminal *6xHIS-3xFLAG* tag. To generate the plasmid vectors, we used the Phusion High-Fidelity PCR Kit (New England Biolabs, Frankfurt, Germany). All plasmid DNA vectors were maintained and were amplified in *E. coli* TOP10F′ (Thermo Fisher Scientific, Schwerte, Germany). Plasmid vector sequences were verified by sequencing (GATC Biotech, Cologne, Germany).

Production of lentiviral particles

We generated lentiviral particles as described previously (Schmidtke et al., 2017). Briefly, a lentiviral expression plasmid vector, the envelope plasmid vector pMD2.G, and the packaging plasmid vector psPAX2 were co-transfected into HEK293T cells using polyethylenimine (linear PEI; MW 25,000; Polysciences Europe, Eppelheim, Germany). The plasmid vectors pMD2.G and psPAX2 were Addgene plasmids #12259 and #12260 (deposited by Didier Trono). After 8–16 h, the culture medium was refreshed. The cell culture supernatant containing the lentiviral particles was collected 48 h and 72 h after transfection. Prior to purification of the lentiviral particles, remaining vector DNA in the supernatant was removed by digestion with DNase I (Roche/Sigma-Aldrich, Munich, Germany). After sterile-filtration (0.45 µm, PES membrane; VWR/TPP, Bruchsal, Germany), the lentiviral particles were concentrated by polyethylene glycol 6000 (PEG6,000; Carl Roth, Karlsruhe, Germany) precipitation. We dissolved the purified lentiviral particles in PBS and stored working aliquots at −80°C. To determine titres of lentiviral preparations, HEK293T cells were transduced with tenfold serial dilutions of the purified lentiviral particles. We calculated functional titres based on the percentage of GFP-positive cells measured by flow cytometry. Vehicle control (GFP only) lentiviral particles were generated using the plasmid vector pCDH-CMV-MCS-EF1α-copGFP since the copGFP gene is under the direct control of the EF1α promoter.

Transduction of cells

We transduced murine BMDCs at a multiplicity of infection (MOI) of 50 by spinfection on day 4 of differentiation. The BMDCs were harvested and 2×10^6 cells distributed into bacteriological six-well plates (Carl Roth, Karlsruhe, Germany) in complete RPMI 1640. We first mixed the lentiviral

Journal of Cell Science (2020) 133, jcs240085. doi:10.1242/jcs.240085

particles with protamine sulphate (MP Biomedicals, Illkirch, France) and then added this transduction mix to the BMDCs. The volume was adjusted to 2 ml with complete RPMI 1640 to get a final concentration of 50 µg/ml protamine sulfate. Mock-transduced cells received complete RPMI 1640 with protamine sulfate instead of lentiviral particles. Finally, the six-well plates with the BMDCs in the transduction mix were centrifuged at 32°C for 90 min and 1500 ***g***. After centrifugation, we resuspended and transferred the BMDCs back into bacteriological 10 cm Petri dishes. The BMDCs were cultured further in a final volume of 10 ml of complete RPMI 1640. On day 6, we added 10 ml of complete RPMI 1640, and refreshed half of the culture medium with complete RPMI 1640 on day 8. On day 10, we seeded the BMDCs appropriately for experiments. Successful transduction was tested by flow cytometry, measuring GFP-positive cells. The transduction efficiency was determined prior to seeding of the BMDCs for experiments on day 9 or 10 of culture. HeLa cells (10^6) were transduced at an MOI of 25–30 in 10 cm dishes. Again, we mixed lentiviral particles with protamine sulfate (final concentration 50 µg/ml), and added the transduction mix subsequently to the cells. The HeLa cells were incubated with the transduction mix for 3 days. On day 3, we seeded the HeLa cells appropriately for use in confocal microscopy and left the cells to adhere overnight. To induce aggresome formation, HeLa cells were treated with 10 µM MG132 for 6 h prior to fixation. To test successful transduction, the percentage of GFP-positive cells was measured by flow cytometry. Transduction efficiency was determined prior to seeding of cells for experiments on day 3 post-transduction.

Confocal microscopy

Cells were seeded on poly-L-lysine-coated (Sigma-Aldrich, Munich, Germany) coverslips (Menzel-Gläser, diameter 13 mm, thickness #1; VWR, Bruchsal, Germany). At indicated time points, we fixed the cells with 4% paraformaldehyde (Merck, Darmstadt, Germany) in PBS supplemented with 1 mM $MgCl_2$ and 0.1 mM $CaCl_2$ (D-PBS; Carl Roth, Karlsruhe, Germany) for 15 min at RT. Afterwards, the fixed cells were quenched with 50 mM NH_4Cl in D-PBS for 10 min at 4°C and permeabilised using 0.2% Triton X-100 in D-PBS for 5 min at RT. After each step, we washed the cells two to three times with D-PBS. Fixed cells were blocked using 1× Roti-ImmunoBlock (Carl Roth, Karlsruhe, Germany) or 0.2% fish-skin gelatine (Sigma-Aldrich, Munich, Germany) in D-PBS (blocking buffer). All immunostainings were incubated for 60 min at RT. We used the following primary antibodies: mouse anti-FAT10 (4F1; 1 µg/ml; Aichem et al., 2010), rabbit anti-ubiquitin (10H4L21; 2.5 µg/ml; Cat. No. 701339, Thermo Fisher Scientific, Schwerte, Germany), unconjugated and biotinylated mouse anti-ubiquitin (FK2; 1 µg/ml; Cat. Nos. BML-PW8810 and BML-PW0755, Enzo Life Sciences, Lörrach, Germany), rabbit anti-p62 (H290; 1 µg/ml; Cat. No. sc-25575, Santa Cruz Biotechnology, Heidelberg, Germany), and mouse anti-FLAG (M2; 0.5 µg/ml; Cat. No. F3165, Sigma-Aldrich, Munich, Germany). After washing with D-PBS, we incubated the cells with appropriate secondary antibodies (4 µg/ml), which were F(ab')2-goat anti-rabbit or -mouse IgG fragments coupled to Alexa Fluor-488, -546 or -568, and -647 or streptavidin coupled to eFluor570 (Cat. Nos. A-11017, A-11071, A-11019, A-21246, Thermo Fisher Scientific, Schwerte, Germany). We diluted all antibodies in blocking buffer. For mounting of coverslips onto microscopy slides, we used DAPI Fluoromount-G (SouthernBiotech, Birmingham, USA). Images were acquired using a Zeiss LSM510 Meta or LSM880 confocal laser-scanning microscope (Carl Zeiss, Jena, Germany) with a 40× or 63× plan-apochromat, oil-immersion objective (both with NA 1.4). We analysed images using ImageJ FIJI software version 1.51s (Schindelin et al., 2012) and its feature 'analyse particles'. To avoid false positives from nuclei, we depleted the DAPI signals prior to analysis. For counting, the intensity threshold of the image was set as high as possible to avoid noise. Additionally, we compared threshold-adjusted images with original images to avoid false-positive DALIS. In this way, particles that were counted by the software, but were positioned outside of the cells, were excluded from analysis. The size cut-off for counting DALIS was set to 0.15–infinity µm². To determine the Pearson's coefficient, region of interests (ROIs) of DALIS were defined in images of 0.8 mm thickness and ImageJ software (coloc2 plugin) was used to measure the Pearson's correlation above threshold.

Quantitative real-time RT-PCR

To evaluate gene expression, we extracted total RNA with the RNeasy Plus Mini Kit (QIAGEN, Hilden, Germany) according to the manufacturer's instruction. cDNA was synthesised from total RNA using the Reverse Transcription System (Promega, Mannheim, Germany) or the High Capacity cDNA Reverse Transcription Kit (Applied Biosystems/Thermo Fisher Scientific, Schwerte, Germany). The level of expression was measured using the LightCycler FastStart DNA Master SYBR Green I Kit (Roche, Mannheim, Germany) or the Fast SYBR Green Master Mix (Applied Biosystems/Thermo Fisher Scientific, Schwerte, Germany). For analysis, we used the LightCycler instrument with the LightCycler Software Version 3.5 (both from Roche, Mannheim, Germany), the TOptical Gradient 96 Real-Time PCR-Thermocycler and the qPCRsoft V3.1 software (both from Analytik Jena, Jena, Germany), or the 7900HT Fast Real-time PCR System and the Sequence Detection Systems software version 2.4.1 (both from Applied Biosystems/Thermo Fisher Scientific, Schwerte, Germany). The primers used for qPCR are listed in Table S1. The PCR programs in the LightCycler software and the qPCRsoft V3.1 software were set up identically and have been described previously (Buerger et al., 2015). PCR conditions for the use of the Fast SYBR Green Master Mix were as follows: initial denaturation at 95°C for 20 s followed by 40 cycles of denaturation at 95°C for 1 s, and annealing and elongation at 60°C for 20 s. We calculated the relative expression level using the Excel-based relative expressions software tool with a multiple condition solver (REST-MCS) version 2 according to the Pfaffl method (Pfaffl et al., 2002).

Flow cytometry

We assessed the phenotype and the proper maturation of DCs by cell surface staining using the following antibodies (clone): anti-CD11c (3.9), Cat. No. 11-0116-42, anti-CD83 (HB15e), Cat. No. 551073, and anti-CD86 (2331/FUN-1), Cat. No. 555658, on human MoDCs and anti-CD11c (HL3), Cat. No. 550261, anti-CD86 (GL1), Cat. No. 553692, and anti-MHC class II (I-A/I-E) (M5/114.15.2), Cat. No. 12-5321-82, on murine BMDCs. Antibodies were purchased from BD Biosciences (Heidelberg, Germany) or Thermo Fisher Scientific (Schwerte, Germany). The cells were pelleted, washed with PBS supplemented with 2% iFCS and 2 mM EDTA (FACS buffer), and were incubated for 10 min at 4°C with Fc block diluted in FACS buffer in order to prevent unspecific binding. We used self-made Fc block (supernatant of hybridoma 2.4G2) for BMDCs and incubated MoDCs with commercially available Fc block (Miltenyi Biotec, Bergisch Gladbach, Germany). Mouse IgG_1, κ (P3.6.2.8.1), Cat. No. 11-4714-42, was used as isotype control for MoDCs and hamster IgG_1, λ1 (G235-2356), Cat. No. 553956, and rat IgG_{2a}, κ (eBR2a), Cat. No. 12-4321-42, for BMDCs. All antibodies used in flow cytometry were diluted in FACS buffer. Without washing, we incubated the blocked cells with antibodies for 20 min at 4°C using a 1:200 dilution, followed by two to three washing steps with FACS buffer. We acquired fluorescence signals using an Accuri C6, a FACSCalibur, or a LSR II flow cytometer (all from BD Biosciences, Heidelberg, Germany). Monocyte-derived dendritic cells were stained additionally with TO-PRO-3 (Thermo Fisher Scientific, Schwerte, Germany) in order to assess the viability of the cells.

SDS-PAGE and western blot analysis

We prepared whole-cell lysates in RIPA lysis buffer (50 mM Tris-HCl pH 7.4, 150 mM NaCl, 1% Triton X-100, 1% sodium deoxycholate, 0.1% SDS, 1 mM EDTA) supplemented with 1× protease inhibitor cocktail (complete Mini EDTA-free) (Roche, Mannheim, Germany). For lysis, cells were resuspended in lysis buffer, incubated on ice for 30 min, and vortexed every 10 min. Lysates were cleared by ultracentrifugation at 20,000 ***g*** at RT for 5 min. Finally, protein concentrations were determined using the Pierce BCA protein assay kit (Thermo Fisher Scientific, Schwerte, Germany). Protein levels were adjusted to be equal in each sample. Following adjustment of protein concentrations, total cell lysates were boiled with 5× SDS sample buffer (225 mM Tris-HCl pH 6.8, 50% glycerol, 5% SDS, 0.05% bromophenol blue) supplemented with 4% β-mercaptoethanol at 95°C for 5 min. Protein samples were separated by SDS-PAGE under denaturing conditions using the Tetra cell system (Bio-Rad, Feldkirchen, Germany). We used 10% gels for SDS-PAGE and ran them using the

discontinuous Laemmli buffer system. After separation, proteins were transferred onto Amersham Protran 0.45 NC nitrocellulose membranes (GE Healthcare, Freiburg, Germany) using a semidry blotter (Hoefer/VWR, Bruchsal, Germany) and the discontinuous buffer system ROTI® Blot1. Membranes were rinsed with double-distilled H_2O and blocked at RT for 30–60 min in 1× Roti-Block in PBS containing 0.2% Tween20 (PBS-T). Following blocking, membranes were incubated with primary antibodies against p62 (1:1000; guinea pig polyclonal serum GP62-C, Cat. No. GP62-C, from PROGEN, Heidelberg, Germany) and, as a loading control, against β-actin (1:5000; clone AC-15, Cat. No. ab2676, from Abcam, Berlin, Germany) at RT for 2 h or at 4°C overnight. After washing, membranes were incubated with IRDye 800CW-coupled anti-guinea pig (Cat. No. 925-32411) and IRDye680RD-coupled anti-mouse secondary antibody (Cat. No. 926-68070) at RT for 2 h diluted at 1:15,000. Antibodies were diluted in 1× Roti-Block in PBS. Secondary antibodies, the western blot imaging system 'Odyssey Fc', and the Image Studio software version 5.2 for analysis of western blots were purchased from LI-COR Biosciences, Bad Homburg, Germany. Unless otherwise stated, all buffers and reagents for SDS-PAGEs and western blotting were purchased from Carl Roth (Karlsruhe, Germany), Sigma-Aldrich (Munich, Germany) and AppliChem (Darmstadt, Germany).

Statistical analysis

To analyse the data statistically, we used the GraphPad Prism 6 software (version 6.04) (GraphPad Software, La Jolla, USA). For statistical comparison, we applied either the two-tailed paired *t*-test or the repeated-measures (RM) one-way ANOVA with the Geisser–Greenhouse correction. Following the RM one-way ANOVA, planned multiple comparisons were analysed by use of an uncorrected Fisher's LSD test.

Acknowledgements

We are grateful to Gabriele Matthias and Patrick Matthias (Friedrich Miescher Institute for Biomedical Research, Basel, Switzerland) for providing hind legs of WT and HDAC6-deficient mice. We thank Gunter Schmidtke (University of Konstanz, Konstanz, Germany) for his advice as well as discussions, and Ilona Kindinger (Biotechnology Institute Thurgau at the University of Konstanz, Kreuzlingen, Switzerland) for her experimental support. We acknowledge the support from the personnel of the Flow Cytometry Centre, the Bioimaging Center, and the Animal Research Facility of the University of Konstanz.

Competing interests

The authors declare no competing or financial interests.

Author contributions

Conceptualization: R.S., M.G.; Methodology: R.S., S.M., D.F.L., J.R., W.A.K.; Software: R.S.; Validation: R.S., M.G.; Formal analysis: R.S., M.G.; Investigation: R.S., S.M.; Resources: D.F.L., J.R., M.G.; Data curation: M.G.; Writing - original draft: R.S.; Writing - review & editing: D.F.L., J.R., M.G.; Supervision: J.R., M.G.; Project administration: W.A.K., D.F.L., J.R., M.G.; Funding acquisition: D.F.L., J.R., M.G.

Funding

This project was financially supported by Deutsche Forschungsgemeinschaft CRC969 Project C01 and grant GR 1517/25-1.

Supplementary information

Supplementary information available online at
https://jcs.biologists.org/lookup/doi/10.1242/jcs.240085.supplemental

Peer review history

The peer review history is available online at
https://jcs.biologists.org/lookup/doi/10.1242/jcs.240085.reviewer-comments.pdf

References

Aichem, A., Pelzer, C., Lukasiak, S., Kalveram, B., Sheppard, P. W., Rani, N., Schmidtke, G. and Groettrup, M. (2010). USE1 is a bispecific conjugating enzyme for ubiquitin and FAT10, which FAT10ylates itself in cis. *Nat. Commun.* **1**, 13. doi:10.1038/ncomms1012

Aichem, A., Kalveram, B., Spinnenhirn, V., Kluge, K., Catone, N., Johansen, T. and Groettrup, M. (2012). The proteomic analysis of endogenous FAT10 substrates identifies p62/SQSTM1 as a substrate of FAT10ylation. *J. Cell Sci.* **125**, 4576–4585. doi:10.1242/jcs.107789

Aichem, A., Catone, N. and Groettrup, M. (2014). Investigations into the auto-FAT10ylation of the bispecific E2 conjugating enzyme UBA6-specific E2 enzyme 1. *FEBS J.* **281**, 1848–1859. doi:10.1111/febs.12745

Alloatti, A., Kotsias, F., Magalhaes, J. G. and Amigorena, S. (2016). Dendritic cell maturation and cross-presentation: timing matters! *Immunol. Rev.* **272**, 97–108.

Argüello, R. J., Reverendo, M., Gatti, E. and Pierre, P. (2016). Regulation of protein synthesis and autophagy in activated dendritic cells: implications for antigen processing and presentation. *Immunol. Rev.* **272**, 28–38. doi:10.1111/imr.12427

Basler, M., Buerger, S. and Groettrup, M. (2015). The ubiquitin-like modifier FAT10 in antigen processing and antimicrobial defense. *Mol. Immunol.* **68**, 129–132. doi:10.1016/j.molimm.2015.04.012

Bates, E. E. M., Ravel, O., Dieu, M. C., Ho, S., Guret, C., Bridon, J. M., Ait-Yahia, S., Brière, F., Caux, C., Banchereau, J. et al. (1997). Identification and analysis of a novel member of the ubiquitin family expressed in dendritic cells and mature B cells. *Eur. J. Immunol.* **27**, 2471–2477. doi:10.1002/eji.1830271002

Bialas, J., Groettrup, M. and Aichem, A. (2015). Conjugation of the ubiquitin activating enzyme UBE1 with the ubiquitin-like modifier FAT10 targets it for proteasomal degradation. *PLoS One* **10**, e0120329. doi:10.1371/journal.pone.0120329

Bjørkøy, G., Lamark, T., Brech, A., Outzen, H., Perander, M., Øvervatn, A., Stenmark, H. and Johansen, T. (2005). p62/SQSTM1 forms protein aggregates degraded by autophagy and has a protective effect on huntingtin-induced cell death. *J. Cell Biol.* **171**, 603–614. doi:10.1083/jcb.200507002

Buerger, S., Herrmann, V. L., Mundt, S., Trautwein, N., Groettrup, M. and Basler, M. (2015). The Ubiquitin-like Modifier FAT10 Is Selectively Expressed in Medullary Thymic Epithelial Cells and Modifies T Cell Selection. *J. Immunol.* **195**, 4106–4116. doi:10.4049/jimmunol.1500592

Canaan, A., Yu, X., Booth, C. J., Lian, J., Lazar, I., Gamfi, S. L., Castille, K., Kohya, N., Nakayama, Y., Liu, Y.-C. et al. (2006). FAT10/Diubiquitin-Like Protein-Deficient Mice Exhibit Minimal Phenotypic Differences. *Mol. Cell. Biol.* **26**, 5180–5189. doi:10.1128/MCB.00966-05

Canadien, V., Tan, T., Zilber, R., Szeto, J., Perrin, A. J. and Brumell, J. H. (2005). Cutting Edge: Microbial Products Elicit Formation of Dendritic Cell Aggresome-Like Induced Structures in Macrophages. *J. Immunol.* **174**, 2471–2475. doi:10.4049/jimmunol.174.5.2471

Cenci, S., Mezghrani, A., Cascio, P., Bianchi, G., Cerruti, F., Fra, A., Lelouard, H., Masciarelli, S., Mattioli, L., Oliva, L. et al. (2006). Progressively impaired proteasomal capacity during terminal plasma cell differentiation. *EMBO J.* **25**, 1104–1113. doi:10.1038/sj.emboj.7601009

Ceppi, M., Clavarino, G., Gatti, E., Schmidt, E. K., De Gassart, A., Blankenship, D., Ogola, G., Banchereau, J., Chaussabel, D. and Pierre, P. (2009). Ribosomal protein mRNAs are translationally-regulated during human dendritic cells activation by LPS. *Immunome Res.* **5**, 5. doi:10.1186/1745-7580-5-5

Chiu, Y. H., Sun, Q. and Chen, Z. J. (2007). E1-L2 Activates Both Ubiquitin and FAT10. *Mol. Cell* **27**, 1014–1023. doi:10.1016/j.molcel.2007.08.020

DeFillipo, A. M., Dai, J. and Li, Z. (2004). Heat shock-induced dendritic cell maturation is coupled by transient aggregation of ubiquitinated proteins independently of heat shock factor 1 or inducible heat shock protein 70. *Mol. Immunol.* **41**, 785–792. doi:10.1016/j.molimm.2004.04.016

Ebstein, F., Lange, N., Urban, S., Seifert, U., Krüger, E. and Kloetzel, P. M. (2009). Maturation of human dendritic cells is accompanied by functional remodelling of the ubiquitin-proteasome system. *Int. J. Biochem. Cell Biol.* **41**, 1205–1215. doi:10.1016/j.biocel.2008.10.023

Ebstein, F., Lehmann, A. and Kloetzel, P. M. (2012). The FAT10- and ubiquitin-dependent degradation machineries exhibit common and distinct requirements for MHC class I antigen presentation. *Cell. Mol. Life Sci.* **69**, 2443–2454. doi:10.1007/s00018-012-0933-5

Fan, W., Liu, Y. C., Parimoo, S. and Weissman, S. M. (1995). Olfactory receptor-like genes are located in the human major histocompatibility complex. *Genomics* **27**, 119–123. doi:10.1006/geno.1995.1013

Fan, W., Cai, W., Parimoo, S., Lennon, G. G. and Weissman, S. M. (1996). Identification of seven new human MHC class I region genes around the HLA-F locus. *Immunogenetics* **44**, 97–103. doi:10.1007/BF02660056

Faßbender, M., Herter, S., Holtappels, R. and Schild, H. (2008). Correlation of dendritic cell maturation and the formation of aggregates of poly-ubiquitinated proteins in the cytosol. *Med. Microbiol. Immunol.* **197**, 185–189. doi:10.1007/s00430-008-0091-4

Fujita, K.-I., Maeda, D., Xiao, Q. and Srinivasula, S. M. (2011). Nrf2-mediated induction of p62 controls Toll-like receptor-4-driven aggresome-like induced structure formation and autophagic degradation. *Proc. Natl. Acad. Sci. U.S.A.* **108**, 1427–1432. doi:10.1073/pnas.1014156108

Gu, X., Zhao, F., Zheng, M., Fei, X., Chen, X., Huang, S., Xie, Y. and Mao, Y. (2007). Cloning and characterization of a gene encoding the human putative ubiquitin conjugating enzyme E2Z (UBE2Z). *Mol. Biol. Rep.* **34**, 183–188. doi:10.1007/s11033-006-9033-7

Herter, S., Osterloh, P., Hilf, N., Rechtsteiner, G., Höhfeld, J., Rammensee, H.-G. and Schild, H. (2005). Dendritic Cell Aggresome-Like-Induced Structure Formation and Delayed Antigen Presentation Coincide in Influenza Virus-Infected Dendritic Cells. *J. Immunol.* **175**, 891–898. doi:10.4049/jimmunol.175.2.891

Hipp, M. S., Kalveram, B., Raasi, S., Groettrup, M. and Schmidtke, G. (2005). FAT10, a ubiquitin-independent signal for proteasomal degradation. *Mol. Cell. Biol.* **25**, 3483–3491. doi:10.1128/MCB.25.9.3483-3491.2005

Hu, H. and Sun, S.-C. (2016). Ubiquitin signaling in immune responses. *Cell Res.* **26**, 457–483. doi:10.1038/cr.2016.40

Jin, J., Li, X., Gygi, S. P. and Harper, J. W. (2007). Dual E1 activation systems for ubiquitin differentially regulate E2 enzyme charging. *Nature* **447**, 1135–1138. doi:10.1038/nature05902

Johnston, J. A., Ward, C. L. and Kopito, R. R. (1998). Aggresomes: A cellular response to misfolded proteins. *J. Cell Biol.* **143**, 1883–1898. doi:10.1083/jcb.143.7.1883

Joshi, D. C. and Bakowska, J. C. (2011). Spg20 protein spartin associates with cardiolipin via its plant-related senescence domain and regulates mitochondrial ca^{2+} homeostasis. *PLoS One* **6**, e19290. doi:10.1371/journal.pone.0019290

Kalveram, B., Schmidtke, G. and Groettrup, M. (2008). The ubiquitin-like modifier FAT10 interacts with HDAC6 and localizes to aggresomes under proteasome inhibition. *J. Cell Sci.* **121**, 4079–4088. doi:10.1242/jcs.035006

Kaniuk, N. A., Kiraly, M., Bates, H., Vranic, M., Volchuk, A. and Brumell, J. H. (2007). Ubiquitinated-protein aggregates form in pancreatic β-cells during diabetes-induced oxidative stress and are regulated by autophagy. *Diabetes* **56**, 930–939. doi:10.2337/db06-1160

Karlsson, A. B., Washington, J., Dimitrova, V., Hooper, C., Shekhtman, A. and Bakowska, J. C. (2014). The role of spartin and its novel ubiquitin binding region in DALIS occurrence. *Mol. Biol. Cell* **25**, 1355-1365. doi:10.1091/mbc.e13-11-0705

Kawaguchi, Y., Kovacs, J. J., McLaurin, A., Vance, J. M., Ito, A. and Yao, T.-P. (2003). The deacetylase HDAC6 regulates aggresome formation and cell viability in response to misfolded protein stress. *Cell* **115**, 727–738. doi:10.1016/S0092-8674(03)00939-5

Kerscher, O., Felberbaum, R. and Hochstrasser, M. (2006). Modification of Proteins by Ubiquitin and Ubiquitin-Like Proteins. *Annu. Rev. Cell Dev. Biol.* **22**, 159–180. doi:10.1146/annurev.cellbio.22.010605.093503

Kettern, N., Rogon, C., Limmer, A., Schild, H. and Höhfeld, J. (2011). The Hsc/Hsp70 co-chaperone network controls antigen aggregation and presentation during maturation of professional antigen presenting cells. *PLoS One* **6**, e16398. doi:10.1371/journal.pone.0016398

Khan, S., de Giuli, R., Schmidtke, G., Bruns, M., Buchmeier, M., van den Broek, M. and Groettrup, M. (2001). Cutting Edge: Neosynthesis Is Required for the Presentation of a T Cell Epitope from a Long-Lived Viral Protein. *J. Immunol.* **167**, 4801–4804. doi:10.4049/jimmunol.167.9.4801

Kondylis, V., Van Nispen Tot Pannerden, H. E., Van Dijk, S., Ten Broeke, T., Wubbolts, R., Geerts, W. J., Seinen, C., Mutis, T. and Heijnen, H. F. G. (2013). Endosome-mediated autophagy: An unconventional MIIC-driven autophagic pathway operational in dendritic cells. *Autophagy* **9**, 861–880. doi:10.4161/auto.24111

Kopito, R. R. (2000). Aggresomes, inclusion bodies and protein aggregation. *Trends Cell Biol.* **10**, 524–530. doi:10.1016/S0962-8924(00)01852-3

Lamark, T. and Johansen, T. (2012). Aggrephagy: Selective disposal of protein aggregates by macroautophagy. *Int. J. Cell Biol.* **736905**, 21.

Lee, C. G., Ren, J., Cheong, I. S., Ban, K. H., Ooi, L. L., Yong Tan, S., Kan, A., Nuchprayoon, I., Jin, R., Lee, K. H. et al. (2003). Expression of the FAT10 gene is highly upregulated in hepatocellular carcinoma and other gastrointestinal and gynecological cancers. *Oncogene* **22**, 2592–2603. doi:10.1038/sj.onc.1206337

Lelouard, H., Gatti, E., Cappello, F., Gresser, O., Camosseto, V. and Pierre, P. (2002). Transient aggregation of ubiquitinated proteins during dendritic cell maturation. *Nature* **417**, 177–182. doi:10.1038/417177a

Lelouard, H., Ferrand, V., Marguet, D., Bania, J., Camosseto, V., David, A., Gatti, E. and Pierre, P. (2004). Dendritic cell aggresome-like induced structures are dedicated areas for ubiquitination and storage of newly synthesized defective proteins. *J. Cell Biol.* **164**, 667–675. doi:10.1083/jcb.200312073

Lelouard, H., Schmidt, E. K., Camosseto, V., Clavarino, G., Ceppi, M., Hsu, H.-T. and Pierre, P. (2007). Regulation of translation is required for dendritic cell function and survival during activation. *J. Cell Biol.* **179**, 1427–1439. doi:10.1083/jcb.200707166

Li, J., Chai, Q.-Y. and Liu, C. H. (2016). The ubiquitin system: a critical regulator of innate immunity and pathogen–host interactions. *Cell. Mol. Immunol.* **13**, 560–576. doi:10.1038/cmi.2016.40

Liu, Y.-C., Pan, J., Zhang, C., Fan, W., Collinge, M., Bender, J. R. and Weissman, S. M. (1999). A MHC-encoded ubiquitin-like protein (FAT10) binds noncovalently to the spindle assembly checkpoint protein MAD2. *Proc. Natl. Acad. Sci. U.S.A.* **96**, 4313–4318. doi:10.1073/pnas.96.8.4313

Liu, X., Wang, Q., Chen, W. and Wang, C. (2013). Dynamic regulation of innate immunity by ubiquitin and ubiquitin-like proteins. *Cytokine Growth Factor. Rev.* **24**, 559–570. doi:10.1016/j.cytogfr.2013.07.002

Lu, J., Rashid, F. and Byrne, P. C. (2006). The hereditary spastic paraplegia protein spartin localises to mitochondria. *J. Neurochem.* **98**, 1908–1919. doi:10.1111/j.1471-4159.2006.04008.x

Lukasiak, S., Schiller, C., Oehlschlaeger, P., Schmidtke, G., Krause, P., Legler, D. F., Autschbach, F., Schirmacher, P., Breuhahn, K. and Groettrup, M. (2008). Proinflammatory cytokines cause FAT10 upregulation in cancers of liver and colon. *Oncogene* **27**, 6068–6074. doi:10.1038/onc.2008.201

Lutz, M. B., Kukutsch, N., Ogilvie, A. L. J., Rößner, S., Koch, F., Romani, N. and Schuler, G. (1999). An advanced culture method for generating large quantities of highly pure dendritic cells from mouse bone marrow. *J. Immunol. Methods* **223**, 77–92. doi:10.1016/S0022-1759(98)00204-X

Mah, M. M., Basler, M. and Groettrup, M. (2019). The ubiquitin-like modifier FAT10 is required for normal IFN-γ production by activated CD^{8+} T cells. *Mol. Immunol.* **108**, 111–120. doi:10.1016/j.molimm.2019.02.010

Mellman, I. (2013). Dendritic Cells: Master Regulators of the Immune Response. *Cancer Immunol. Res.* **1**, 145–149. doi:10.1158/2326-6066.CIR-13-0102

Nathan, J. A., Spinnenhirn, V., Schmidtke, G., Basler, M., Groettrup, M. and Goldberg, A. L. (2013). Immuno- and constitutive proteasomes do not differ in their abilities to degrade ubiquitinated proteins. *Cell* **152**, 1184–1194. doi:10.1016/j.cell.2013.01.037

Ocklenburg, F., Moharregh-Khiabani, D., Geffers, R., Janke, V., Pfoertner, S., Garritsen, H., Groebe, L., Klempnauer, J., Dittmar, K. E. J., Weiss, S. et al. (2006). UBD, a downstream element of FOXP3, allows the identification of LGALS3, a new marker of human regulatory T cells. *Lab. Investig.* **86**, 724–737. doi:10.1038/labinvest.3700432

Oudshoorn, D., Versteeg, G. A. and Kikkert, M. (2012). Regulation of the innate immune system by ubiquitin and ubiquitin-like modifiers. *Cytokine Growth Factor. Rev.* **23**, 273–282. doi:10.1016/j.cytogfr.2012.08.003

Ouyang, H., Ali, Y. O., Ravichandran, M., Dong, A., Qiu, W., MacKenzie, F., Dhe-Paganon, S., Arrowsmith, C. H. and Zhai, R. G. (2012). Protein aggregates are recruited to aggresome by histone deacetylase 6 via unanchored ubiquitin C termini. *J. Biol. Chem.* **287**, 2317–2327. doi:10.1074/jbc.M111.273730

Pelzer, C., Kassner, I., Matentzoglu, K., Singh, R. K., Wollscheid, H.-P., Scheffner, M., Schmidtke, G. and Groettrup, M. (2007). UBE1L2, a novel E1 enzyme specific for ubiquitin. *J. Biol. Chem.* **282**, 23010–23014. doi:10.1074/jbc.C700111200

Pfaffl, M. W., Horgan, G. W. and Dempfle, L. (2002). Relative expression software tool (REST(C)) for group-wise comparison and statistical analysis of relative expression results in real-time PCR. *Nucleic Acids Res.* **30**, e36. doi:10.1093/nar/30.9.e36

Pierre, P. (2005). Dendritic cells, DRiPs, and DALIS in the control of antigen processing. *Immunol. Rev.* **207**, 184–190. doi:10.1111/j.0105-2896.2005.00300.x

Raasi, S., Schmidtke, G., De Giuli, R. and Groettrup, M. (1999). A ubiquitin-like protein which is synergistically inducible by interferon-gamma and tumor necrosis factor-alpha. *Eur. J. Immunol.* **29**, 4030–4036. doi:10.1002/(SICI)1521-4141(199912)29:12<4030::AID-IMMU4030>3.0.CO;2-Y

Raasi, S., Schmidtke, G. and Groettrup, M. (2001). The Ubiquitin-like Protein FAT10 Forms Covalent Conjugates and Induces Apoptosis. *J. Biol. Chem.* **276**, 35334–35343. doi:10.1074/jbc.M105139200

Rahnefeld, A., Ebstein, F., Albrecht, N., Opitz, E., Kuckelkorn, U., Stangl, K., Rehm, A., Kloetzel, P. M. and Voigt, A. (2011). Antigen-presentation capacity of dendritic cells is impaired in ongoing enterovirus myocarditis. *Eur. J. Immunol.* **41**, 2774–2781. doi:10.1002/eji.201041039

Rani, N., Aichem, A., Schmidtke, G., Kreft, S. G. and Groettrup, M. (2012). FAT10 and NUB1L bind to the VWA domain of Rpn10 and Rpn1 to enable proteasome-mediated proteolysis. *Nat. Commun.* **3**, 477. doi:10.1038/ncomms1752

Renvoisé, B., Parker, R. L., Yang, D., Bakowska, J. C., Hurley, J. H. and Blackstone, C. (2010). SPG20 protein spartin is recruited to midbodies by ESCRT-III protein Ist1 and participates in cytokinesis. *Mol. Biol. Cell* **21**, 3293–3303. doi:10.1091/mbc.e09-10-0879

Schindelin, J., Arganda-Carreras, I., Frise, E., Kaynig, V., Longair, M., Pietzsch, T., Preibisch, S., Rueden, C., Saalfeld, S., Schmid, B. et al. (2012). Fiji: An open-source platform for biological-image analysis. *Nat. Methods* **9**, 676–682. doi:10.1038/nmeth.2019

Schliehe, C., Bitzer, A., van den Broek, M. and Groettrup, M. (2012). Stable Antigen Is Most Effective for Eliciting $CD8^+$ T-Cell Responses after DNA Vaccination and Infection with Recombinant Vaccinia Virus In Vivo. *J. Virol.* **86**, 9782–9793. doi:10.1128/JVI.00694-12

Schmidtke, G., Kalveram, B. and Groettrup, M. (2009). Degradation of FAT10 by the 26S proteasome is independent of ubiquitylation but relies on NUB1L. *FEBS Lett.* **583**, 591–594. doi:10.1016/j.febslet.2009.01.006

Schmidtke, G., Aichem, A. and Groettrup, M. (2014). FAT10ylation as a signal for proteasomal degradation. *Biochim. Biophys. Acta - Mol. Cell Res.* **1843**, 97–102. doi:10.1016/j.bbamcr.2013.01.009

Schmidtke, G., Schregle, R., Alvarez, G., Huber, E. M. and Groettrup, M. (2017). The 20S immunoproteasome and constitutive proteasome bind with the same affinity to PA28αβ and equally degrade FAT10. *Mol. Immunol.*, **113**, 22–30, https://doi.org/10.1016/j.molimm.2017.11.030

Schregle, R., Mah, M. M., Mueller, S., Aichem, A., Basler, M. and Groettrup, M. (2018). The expression profile of the ubiquitin-like modifier FAT10 in immune cells suggests cell type-specific functions. *Immunogenetics* **70**, 429–438. doi:10.1007/s00251-018-1055-5

Seifert, U., Bialy, L. P., Ebstein, F., Bech-Otschir, D., Voigt, A., Schröter, F., Prozorovski, T., Lange, N., Steffen, J., Rieger, M. et al. (2010). Immunoproteasomes preserve protein homeostasis upon interferon-induced oxidative stress. *Cell* **142**, 613–624. doi:10.1016/j.cell.2010.07.036

Spinnenhirn, V. (2014). Functional analysis of the ubiquitin-like modifier FAT10 in autophagy. *PhD Thesis*, Univ. Konstanz.

Spinnenhirn, V., Farhan, H., Basler, M., Aichem, A., Canaan, A. and Groettrup, M. (2014). The ubiquitin-like modifier FAT10 decorates autophagy-targeted Salmonella and contributes to Salmonella resistance in mice. *J. Cell Sci.* **127**, 4883–4893. doi:10.1242/jcs.152371

Spinnenhirn, V., Bitzer, A., Aichem, A. and Groettrup, M. (2017). Newly translated proteins are substrates for ubiquitin, ISG15, and FAT10. *FEBS Lett.* **591**, 186–195. doi:10.1002/1873-3468.12512

Steinman, R. M. and Nussenzweig, M. C. (2002). Avoiding horror autotoxicus: the importance of dendritic cells in peripheral T cell tolerance. *Proc. Natl. Acad. Sci. U.S.A.* **99**, 351–358. doi:10.1073/pnas.231606698

Szeto, J., Kaniuk, N. A., Canadien, V., Nisman, R., Mizushima, N., Yoshimori, T., Bazett-Jones, D. P. and Brumell, J. H. (2006). ALIS are stress-induced protein storage compartments for substrates of the proteasome and autophagy. *Autophagy* **2**, 189–199. doi:10.4161/auto.2731

Terawaki, S., Camosseto, V., Prete, F., Wenger, T., Papadopoulos, A., Rondeau, C., Combes, A., Rodrigues, C. R., Manh, T. P. V., Fallet, M. et al. (2015). RUN and FYVE domain-containing protein 4 enhances autophagy and lysosome tethering in response to Interleukin-4. *J. Cell Biol.* **210**, 1133–1152. doi:10.1083/jcb.201501059

Wenger, T., Terawaki, S., Camosseto, V., Abdelrassoul, R., Mies, A., Catalan, N., Claudio, N., Clavarino, G., De Gassart, A., Rigotti, F. D. A. et al. (2012). Autophagy inhibition promotes defective neosynthesized proteins storage in ALIS, and induces redirection toward proteasome processing and MHCI-restricted presentation. *Autophagy* **8**, 350–363. doi:10.4161/auto.18806

Yewdell, J. W., Antón, L. C. and Bennink, J. R. (1996). Defective ribosomal products (DRiPs): a major source of antigenic peptides for MHC class I molecules? *J. Immunol.* **157**, 1823–1826.

Zhang, Y., Kwon, S., Yamaguchi, T., Cubizolles, F., Rousseaux, S., Kneissel, M., Cao, C., Li, N., Cheng, H.-L., Chua, K. et al. (2008). Mice Lacking Histone Deacetylase 6 Have Hyperacetylated Tubulin but Are Viable and Develop Normally. *Mol. Cell. Biol.* **28**, 1688–1701. doi:10.1128/MCB.01154-06